

**AFRL-ML-WP-TR-2000-4097**

**EFFECTS OF BALLISTIC IMPACT DAMAGE  
ON FATIGUE CRACK INITIATION IN  
Ti-6Al-4V SIMULATED ENGINE BLADES**



**CAPTAIN CHRISTINE M. MARTINEZ**

**AFRL/MLLN  
CERAMICS DEVELOPMENT AND MATERIALS BEHAVIOR BRANCH  
METALS, CERAMICS AND NDE DIVISION  
WRIGHT-PATTERSON AFB, OH 45433-7750**

**APRIL 2000**

**FINAL REPORT FOR APRIL 2000 – APRIL 2000**

**APPROVED FOR PUBLIC RELEASE; DISTRIBUTION UNLIMITED**

**MATERIALS AND MANUFACTURING DIRECTORATE  
AIR FORCE RESEARCH LABORATORY  
AIR FORCE MATERIEL COMMAND  
WRIGHT-PATTERSON AIR FORCE BASE OH 45433-7750**

## REPORT DOCUMENTATION PAGE

<b>1. REPORT DATE (DD-MM-YYYY)</b> 01-04-2000	<b>2. REPORT TYPE</b> Final Report	<b>3. DATES COVERED (FROM - TO)</b> xx-04-2000 to xx-04-2000
<b>4. TITLE AND SUBTITLE</b> Effects of Ballistic Impact Damage on Fatigue Crack Initiation in Ti-6Al-4V Simulated Engine Blades  Unclassified		<b>5a. CONTRACT NUMBER</b>
		<b>5b. GRANT NUMBER</b>
		<b>5c. PROGRAM ELEMENT NUMBER</b>
<b>6. AUTHOR(S)</b> Martinez, Christine M. ;		<b>5d. PROJECT NUMBER</b>
		<b>5e. TASK NUMBER</b>
		<b>5f. WORK UNIT NUMBER</b>
<b>7. PERFORMING ORGANIZATION NAME AND ADDRESS</b> AFRL/MLLN Ceramics Development and Materials Behavior Branch Metals, Ceramics and NDE Division Wright-Patterson AFB , OH 45433-7750		<b>8. PERFORMING ORGANIZATION REPORT NUMBER</b>
<b>9. SPONSORING/MONITORING AGENCY NAME AND ADDRESS</b> Materials & Manufacturing Directorate Air Force Research Laboratory Air Force Materiel Command Wright-Patterson AFB , OH 45433-7750		<b>10. SPONSOR/MONITOR'S ACRONYM(S)</b>
		<b>11. SPONSOR/MONITOR'S REPORT NUMBER(S)</b>
<b>12. DISTRIBUTION/AVAILABILITY STATEMENT</b> A PUBLIC RELEASE  Materials & Manufacturing Directorate Air Force Research Laboratory Air Force Materiel Command		

Wright-Patterson AFB , OH 45433-7750
<b>13. SUPPLEMENTARY NOTES</b> Thesis submitted to the School of Engineering University of Dayton
<b>14. ABSTRACT</b> This study characterizes damage caused by ballistically impacting spherical glass beads on leading edges of simulated engine blades and correlates it to their high cycle fatigue strength.
<b>15. SUBJECT TERMS</b> high cycle fatigue; turbine engine blades

<b>16. SECURITY CLASSIFICATION OF:</b>			<b>17. LIMITATION OF ABSTRACT</b> Public Release	<b>18. NUMBER OF PAGES</b> 72	<b>19a. NAME OF RESPONSIBLE PERSON</b> Fenster, Lynn lfenster@dtic.mil
<b>a. REPORT</b> Unclassified	<b>b. ABSTRACT</b> Unclassified	<b>c. THIS PAGE</b> Unclassified			<b>19b. TELEPHONE NUMBER</b> International Area Code  Area Code Telephone Number 703 767-9007 DSN 427-9007

## NOTICE

WHEN GOVERNMENT DRAWINGS, SPECIFICATIONS, OR OTHER DATA ARE USED FOR ANY PURPOSE OTHER THAN IN CONNECTION WITH A DEFINITELY GOVERNMENT-RELATED PROCUREMENT, THE UNITED STATES GOVERNMENT INCURS NO RESPONSIBILITY OR ANY OBLIGATION WHATSOEVER. THE FACT THAT THE GOVERNMENT MAY HAVE FORMULATED OR IN ANY WAY SUPPLIED THE SAID DRAWINGS, SPECIFICATIONS, OR OTHER DATA, IS NOT TO BE REGARDED BY IMPLICATION OR OTHERWISE IN ANY MANNER CONSTRUED, AS LICENSING THE HOLDER OR ANY OTHER PERSON OR CORPORATION, OR AS CONVEYING ANY RIGHTS OR PERMISSION TO MANUFACTURE, USE, OR SELL ANY PATENTED INVENTION THAT MAY IN ANY WAY BE RELATED THERETO.

THIS REPORT IS RELEASABLE TO THE NATIONAL TECHNICAL INFORMATION SERVICE (NTIS). AT NTIS, IT WILL BE AVAILABLE TO THE GENERAL PUBLIC, INCLUDING FOREIGN NATIONS.

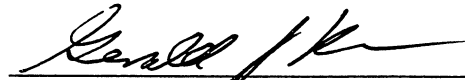
THIS TECHNICAL REPORT HAS BEEN REVIEWED AND IS APPROVED FOR PUBLICATION.



CAPT CHRISTINE M. MARTINEZ  
Ceramics Development & Materials  
Behavior Branch  
Metals, Ceramics & NDE Division



ALLAN P. KATZ, Chief  
Ceramics Development & Materials  
Behavior Branch  
Metals, Ceramics & NDE Division



GERALD J. PETRAK, Asst Chief  
Metals, Ceramics & NDE Division  
Materials & Manufacturing Directorate

COPIES OF THIS REPORT SHOULD NOT BE RETURNED UNLESS RETURN IS REQUIRED BY SECURITY CONSIDERATIONS, CONTRACTUAL OBLIGATIONS, OR NOTICE ON A SPECIFIC DOCUMENT.



REPORT DOCUMENTATION PAGE			Form Approved OMB No. 0704-0188	
Public reporting burden for this collection of information is estimated to average 1 hour per response, including the time for reviewing instructions, searching existing data sources, gathering and maintaining the data needed, and completing and reviewing the collection of information. Send comments regarding this burden estimate or any other aspect of this collection of information, including suggestions for reducing this burden, to Washington Headquarters Services, Directorate for Information Operations and Reports, 1215 Jefferson Davis Highway, Suite 1204, Arlington, VA 22202-4302, and to the Office of Management and Budget, Paperwork Reduction Project (0704-0188), Washington, DC 20503.				
1. AGENCY USE ONLY (Leave blank)		2. REPORT DATE APRIL 2000		3. REPORT TYPE AND DATES COVERED FINAL REPORT FOR APRIL 2000 - APRIL 2000
4. TITLE AND SUBTITLE EFFECTS OF BALLISTIC IMPACT DAMAGE ON FATIGUE CRACK INITIATION IN Ti-6Al-4V SIMULATED ENGINE BLADES			5. FUNDING NUMBERS C IN-HOUSE PE 61102 PR 2302 TA BW WU 1P	
6. AUTHOR(S)  CAPTAIN CHRISTINE M. MARTINEZ				
7. PERFORMING ORGANIZATION NAME(S) AND ADDRESS(ES) AFRL/MLLN CERAMICS DEVELOPMENT AND MATERIALS BEHAVIOR BRANCH METALS, CERAMICS AND NDE DIVISION WRIGHT-PATTERSON AFB, OH 45433-7750			8. PERFORMING ORGANIZATION REPORT NUMBER	
9. SPONSORING/MONITORING AGENCY NAME(S) AND ADDRESS(ES) MATERIALS AND MANUFACTURING DIRECTORATE AIR FORCE RESEARCH LABORATORY AIR FORCE MATERIEL COMMAND WRIGHT-PATTERSON AFB, OH 45433-7750 POC: CAPTAIN CHRISTINE M. MARTINEZ, AFRL/MLLN, 937-255-1347			10. SPONSORING/MONITORING AGENCY REPORT NUMBER  AFRL-ML-WP-TR-2000-4097	
11. SUPPLEMENTARY NOTES THESIS SUBMITTED TO THE SCHOOL OF ENGINEERING UNIVERSITY OF DAYTON				
12a. DISTRIBUTION AVAILABILITY STATEMENT  APPROVED FOR PUBLIC RELEASE, DISTRIBUTION UNLIMITED.			12b. DISTRIBUTION CODE	
13. ABSTRACT (Maximum 200 words)  This study characterizes damage caused by ballistically impacting spherical glass beads on leading edges of simulated engine blades and correlates it to their high cycle fatigue strength. Both leading edges of diamond cross-section tension axial fatigue samples were impacted with 1 mm (0.040") diameter glass beads at 305 m/s (1000 f/s) at an angle of incidence of either 0C or 30C. The samples contained either a sharp leading edge (LE) radius of 0.381 mm (0.015") or a blunt LE radius of 0.127 mm (0.005"). Subsequent fatigue testing showed fatigue strength degradation of 10-50% due to the LE damage, regardless of the depth of the damage zone. Scanning electron microscopy revealed damage features at the fractured notches, including notch depth, loss of material at the notch (LOM), material shear, material folding over the LE, embedded glass from the shattered bead, and microstructural damage. Residual stresses appears to play a role in fatigue strength degradation. In addition, damage on the impact zone seems to contribute to fatigue life degradation as well. Fatigue strength degradation is higher for the 30C impacts than for the 0C impacts. The damage features had no apparent effect on fatigue strength.				
14. SUBJECT TERMS high cycle fatigue, turbine engine blades			15. NUMBER OF PAGES 72	
			16. PRICE CODE	
17. SECURITY CLASSIFICATION OF REPORT  UNCLASSIFIED	18. SECURITY CLASSIFICATION OF THIS PAGE  UNCLASSIFIED	19. SECURITY CLASSIFICATION OF ABSTRACT  UNCLASSIFIED	20. LIMITATION OF ABSTRACT  SAR	



## TABLE OF CONTENTS

LIST OF FIGURES.....	v
LIST OF TABLES.....	viii
LIST OF EQUATIONS .....	viii
ACKNOWLEDGMENTS.....	ix
CHAPTER	
1. INTRODUCTION .....	1
2. MATERIALS AND PROCEDURES.....	7
2.1 MATERIAL PROCESSING.....	7
2.2 SPECIMEN & BALLISTIC IMPACT.....	8
2.3 FATIGUE TESTING .....	11
2.4 NOTCH CHARACTERIZATION.....	13
2.5 SAMPLE POLISHING AND MICRO-SECTIONING.....	17
3. RESULTS AND DISCUSSION.....	19
3.1 TESTING CONDITIONS.....	19
3.1.2 <i>Effects of Angle of Incidence</i> .....	20
3.1.3 <i>Effects of Leading Edge Radius</i> .....	28
3.1.4 <i>Effects of Heat Treatment</i> .....	31
3.2 EFFECTS OF DAMAGE FEATURES .....	36
3.2.1 <i>Effects of Notch Depth</i> .....	36
3.2.2 <i>Effects of Loss of Material (LOM)</i> .....	40
3.2.3 <i>Effects of Microstructural Damage</i> .....	46
3.2.4 <i>Effects of Other Features</i> .....	47
3.3 INITIATION LOCATION IN THE IMPACT NOTCH.....	50
4. CONCLUSIONS.....	52
5. SUGGESTED FUTURE RESEARCH .....	54
6. REFERENCES .....	55
APPENDIX.....	58

A: RAW DATA .....	57
B: ENERGY DISPERSIVE SPECTROSCOPY .....	60

## LIST OF FIGURES

Figure 1: In-service FOD (blades form the F-110-GE-100 engine) .....	2
Figure 2: Borescopes used to inspect engine blades.....	3
Figure 3: General Electric F-110-GE-100 engine <sup>7</sup> .....	4
Figure 4: FOD inspection of F110-GE-100 engine .....	5
Figure 5: Microstructure of Ti-6Al-4V plate material <sup>3</sup> .....	7
Figure 6: Diamond cross-section test specimen, dimensions in inches (mm). <sup>10</sup> .....	8
Figure 7: Schematic of ballistic impact .....	9
Figure 8: Ballistic Impact .....	10
Figure 9: High speed film of 2 mm diameter glass bead impact <sup>12</sup> .....	10
Figure 10: Fatigue step loading procedure <sup>12</sup> .....	12
Figure 11: Un-failed notch for sample 4-22, with a sharp LE and a 30° impact.....	14
Figure 12: Failed notch for sample 4-22.....	15
Figure 13: Fracture views of failed notch for sample 4-22.....	16
Figure 14: a) Illustration of Fractured Sample; b) Top view of mounted sample .....	18
Figure 15: Profile view of mounted sample .....	18
Figure 16: Average normalized fatigue strength of batches 1 through 4 .....	21
Figure 17: Schematic of residual stress fields on ballistic impact sites; a) A head-on 0° impact on a blunt LE; b) An angled impact on a blunt LE, the schematic is based on ref 14.....	22

Figure 18: Postulated residual stress fields on ballistic impact sites; a) A head-on 0° impact on a sharp LE with loss of material; b) A deflected 0° compressing the sharp LE to one side. The schematic is based on ref 14 .....	23
Figure 19: Sharp LE with 0° impacts showing both failed and un-failed notches. ....	25
Figure 20: Blunt LE with 0° impacts showing both failed and un-failed notches.....	26
Figure 21: Samples with 30° impacts showing both failed and un-failed notches. a) Sharp LE; b) Blunt LE .....	27
Figure 22: Notch depth vs. normalized fatigue strength for sharp and blunt LE and for both 0° and 30° impacts.....	29
Figure 23: Loss of Material vs. normalized fatigue strength for sharp and blunt LE and for both 0° and 30° impacts.....	30
Figure 24: Average Normalized Fatigue strength for all testing conditions for 30° impacts. ....	33
Figure 25: Sample 9-1, 30° impact; a) pre-fracture photo, b) post-fracture, c) backscatter detector image of b, d) close-up of b and c. Embedded glass is indicated by the circle, .....	34
Figure 26: Stress relieved samples .....	35
Figure 27: Characteristic Notch Depth (sharp LE with a 30° impact, sample 4-22).....	37
Figure 28: Depth of failed vs. un-failed notches for 0° impacts (sharp and blunt LE)....	37
Figure 29: Depth of failed vs. un-failed notches for 30° impacts (sharp and blunt LE) ..	38

Figure 30: Notch depth vs normalized fatigue strength (sharp and blunt LE).....	39
Figure 31: Loss of Material (sharp LE with a 30° impact, sample 4-22) .....	42
Figure 32: Comparison of materials loss and the fatigue strength; linear squares fit for 0° impacts. (sharp and blunt LE).....	43
Figure 33: LOM for failed vs. un-failed notches for 30° impacts (sharp and blunt LE) .	44
Figure 34: LOM for failed vs. un-failed notches for 0° impacts (sharp and blunt LE) ....	44
Figure 35: Fracture initiation of Sample 3-19 (blunt LE with a 0° impact).....	45
Figure 36: Precision Micro-sectioning of sample 3-13.....	46
Figure 37: Other damage features: a) material shear; b) material shear; c) material fold; d) embedded glass, backscatter detector mode .....	48
Figure 38: Shearing: a) Before fracture picture of sample 3-4 with a blunt LE and a 30° impact, material shear parallel to LE b) After fracture photo; c) After fracture photo behind material shear .....	49
Figure 39: Crack Initiation Location photograph.....	51
Figure 40: Crack Initiation Location.....	51
Figure 41: EDS 1, on glass of sample 4-19, 30° impact on sharp LE. ....	61
Figure 42: EDS 2; 5 µm into the titanium alloy, away from the glass; 30° impact on sharp LE.....	62
Figure 43: EDS 3; 100µm into alloy; 30° impact on sharp LE. ....	63

## LIST OF TABLES

Table 1: Flight-line Serviceability and Repairable limits for F110-GE-100 engine blade leading edges above the root fillet region <sup>2</sup> .....	3
Table 2: Strength Calculation Nomenclature.....	12
Table 3: Samples characterized at the list of each condition .....	19
Table 4: Sample data .....	58

## LIST OF EQUATIONS

Equation 1: Stress Ratio .....	11
Equation 2: Fatigue Strength <sup>10</sup> .....	12
Equation 3: Normalized Fatigue Strength .....	20



## **ACKNOWLEDGMENTS**

I would also like to recognize the members of the 20th Fighter Wing at Shaw AFB who provided a world of insight into FOD inspection in the field; with special thanks to: MSgt Michael Sartain, TSgt David L. Harrington, TSgt Covington, and SSgt Canning.

I would like to also thank Dayton Area Graduate Studies Institute their financial support at the University of Dayton and the High Cycle Fatigue program for providing the research support for this study. Without their support this work would not have been possible.



## **1. INTRODUCTION**

One of the greatest concerns for military and commercial engines is damage caused by the ingestion of foreign debris<sup>1</sup>. This impact damage is known as foreign object damage (FOD). Field experience has shown that FOD results in nicks and dents and reduces life expectancy of those components exposed to vibratory loading<sup>3</sup>. Most of the FOD experienced in the field comes from sand ingestion with depths of about .076 mm (.003") or less. Figure 1 illustrates engine blades with a variety of FOD indicated by the circle. Due to this concern, supplementary FOD inspections and guidelines were implemented into engine maintenance. The guidelines provide instructions of serviceability and repair limits for damaged engine blades, which are based on the depth of the defects<sup>2</sup>. Field FOD inspection is conducted before and after each flight by the maintenance crew chief, in order to prevent catastrophic in-flight failure<sup>4</sup>.

Technical Orders (TO) for both flight-line and engine shop maintenance provide direction on the execution of the FOD inspection as well as serviceability limits for each rotor blade and stator vane in the engine. Limits for FOD found during a flight-line inspection are listed in Table 1. The serviceability limits determine whether the damage needs to be serviced or not. If the damage depth is below the limit noted in the technical order (TO), it is recorded in the maintenance log. If the damage depth exceeds the serviceability limit, it is then

blended out by filing the blade<sup>2</sup>. In addition, if the damage depth exceeds the repairable limit, the engine is pulled out of the aircraft and the blade is replaced. If the FOD depth found on the 1<sup>st</sup> stage fan rotor blade exceeds the serviceability limit shown in Table 1, the 2<sup>nd</sup> and 3<sup>rd</sup> stage rotor blades must be inspected using a device called a borescope, shown in Figure 2. This device utilizes fiber optics in order to view the internal engine components<sup>5</sup>.

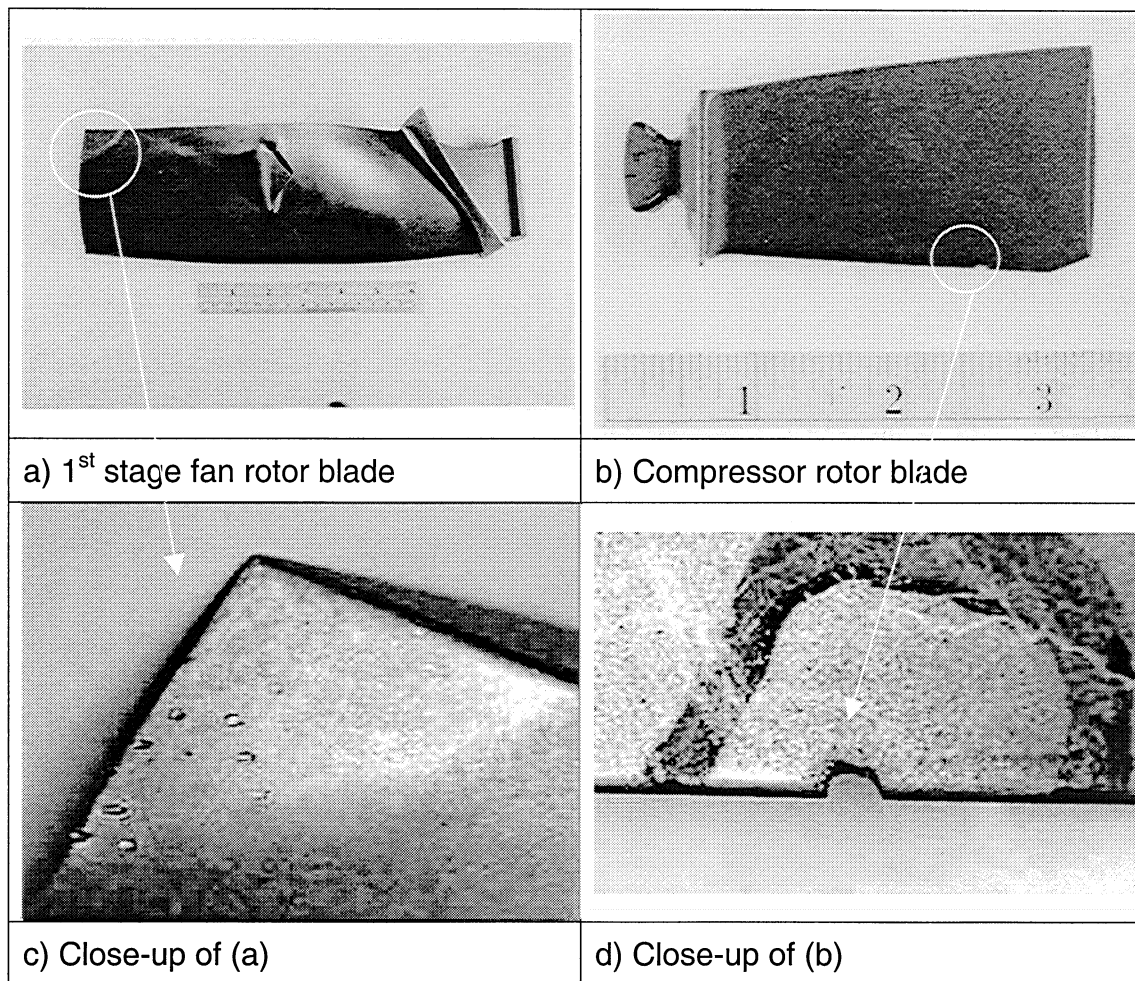


Figure 1: In-service FOD (blades from the F-110-GE-100 engine)

Table 1: Flight-line Serviceability and Repairable limits for F110-GE-100 engine blade leading edges above the root fillet region<sup>2</sup>

Stage	Blade	Serviceable Limit	Repairable Limit
1 <sup>st</sup>	Fan rotor	0.76 mm(0.030")	3.8 mm (0.150")
2 <sup>nd</sup>	Fan rotor	0.76 mm(0.030")	Not repairable/replace blade
3 <sup>rd</sup>	Fan rotor	0.76 mm(0.030")	Not repairable/replace blade
1 <sup>st</sup>	Compressor rotor	0.41 mm(0.016")	Not repairable/replace blade
2 <sup>nd</sup>	Compressor rotor	Data not available <sup>1</sup>	Data not available
3 <sup>rd</sup>	Compressor rotor	Data not available	Data not available
4 <sup>th</sup>	Compressor rotor	0.36 mm(0.014")	Not repairable/replace blade
5 <sup>th</sup>	Compressor rotor	0.36 mm(0.014")	Not repairable/replace blade

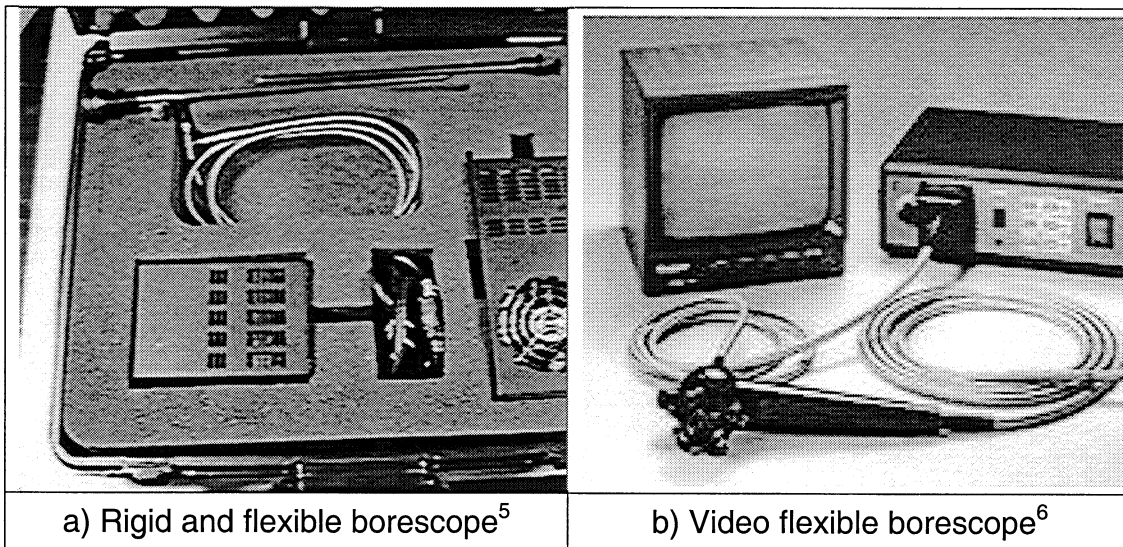


Figure 2: Borescopes used to inspect engine blades

<sup>1</sup> These blades can not be inspected in the flight-line due to borescope entrance restrictions. There are limits in the engine shop TO for all blades.

The current serviceability limit for the first stage fan rotor blade on the F110-GE-129 engine, shown in Figure 3, is 0.76 mm (0.030"). If the damage depth exceeds the maximum repairable limit of 3.8 mm (0.120"), the engine is pulled out of the aircraft for blade replacement<sup>2</sup>. In addition, the entire compressor section must be borescoped, Figure 4a, to determine if there has been further engine FOD damage. Once blade replacement is accomplished, the engine is thoroughly re-inspected, shown in Figure 4b, before returning the engine to operation.

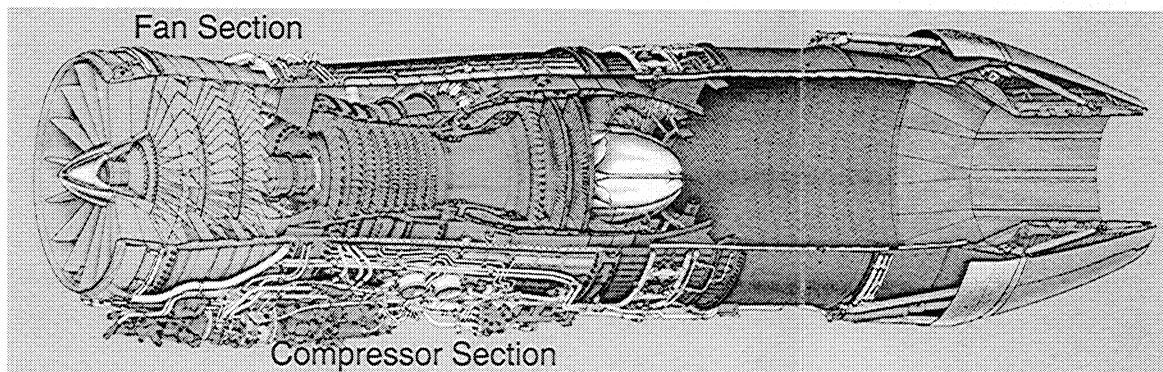


Figure 3: General Electric F-110-GE-100 engine<sup>7</sup>

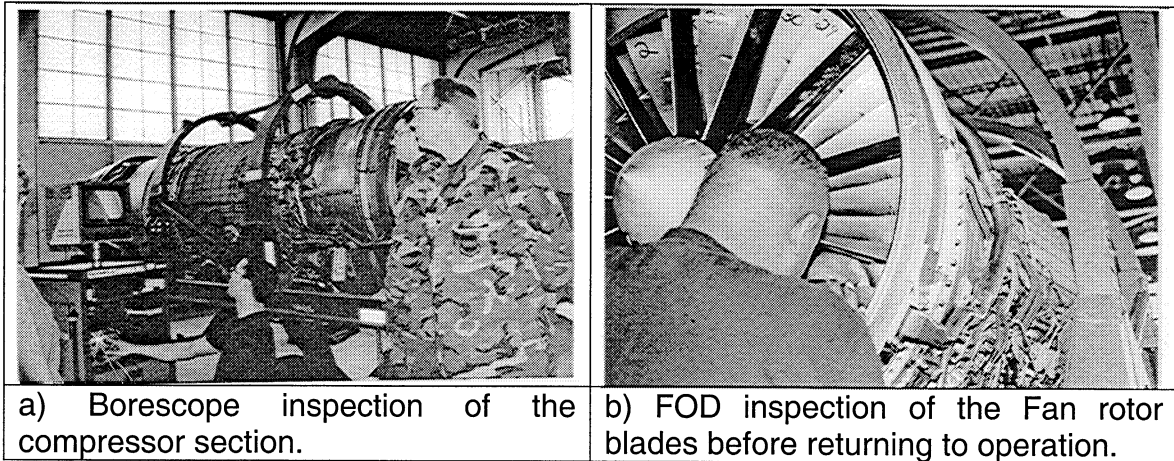


Figure 4: FOD inspection of F110-GE-100 engine

While the maximum serviceable limits for FOD in some jet engines in operation today range from 0.36 to 0.76 mm (0.014" – 0.030"), the damage depths found in this study ranged from 0.068 to 0.427 mm (0.0027" - 0.016"). One item of interest is whether FOD as small as seen in this study provides a significant fatigue strength debit in simulated engine blade specimens. Another item of interest is the determination of whether damage depth is a good indicator of the actual remaining fatigue life of a FOD impacted blade.

Much of the previous impact work has been done on traditional fatigue specimens or rectangular cross-section bars without a leading edge geometry<sup>7,8</sup>. Peters, et al.<sup>7</sup>, researched the effects of FOD on the HCF thresholds by shooting steel spheres onto the flat surface of modified  $K_B$  specimens. This configuration was chosen due to its similarity to the blade loading configuration. They found that the overall effect of FOD markedly reduced the fatigue life compared to that

obtained on undamaged smooth-bar specimens, by providing preferred sites for the premature initiation of fatigue cracks. In addition, Hamrick<sup>8</sup> tested both diamond cross section and uniform rectangular cross section samples to study the effects of FOD. The samples were either ballistically impacted or by quasi-static indentation or shearing. He found that different damage methods created distinctly different damage mechanisms. It was suggested that a total damage depth parameter could be utilized to allow the use of inexpensive and easily controlled methods of simulating FOD, such as the quasi-static chisel indentations, to replace more difficult and expensive means, such as ballistic impacting.

Due to the growing concern of FOD, a study characterizing the damage sites is currently underway in order to understand the effects of FOD on high cycle fatigue strength of engine blades. There are several ways of simulating FOD in a laboratory environment which do provide an impact site and fatigue strength debit; however, each method produces different types of damage which could lead to different crack initiation mechanisms. Characteristic material, geometries representing the leading edge of engine blades and 'realistic' impact conditions were selected for this research. The goal of this research is to quantify the various measurable damage parameters and to determine if they play a role in controlling the fatigue strength in Ti-6Al-4V simulated blades.



## 2. MATERIALS AND PROCEDURES

### 2.1 Material Processing

The samples used in this research were machined from Ti-6Al-4V forgings representative of in-service turbine engine blades. The material was melted and converted to a 6.35 cm (2.5 ") diameter billet followed by mill annealing at 704°C (1300°F) for 2 hours and air cooled in accordance with AMS 4928<sup>11</sup>. The billet was then sectioned into forging multiples, 40.65 cm (16") in length which were preheated to 938°C (1720°F) for up to one hour prior to being pressed into their final forging dimensions of 40.64 X 15.24 X 2.03 cm (16 X 6 X 0.8")<sup>11</sup>. The forgings were air-cooled off the press. This processing resulted in a microstructure consisting of 50 vol% of equiaxed primary alpha with an average 20µm grain-size and a 50 vol% of small colonies of lamellar alpha<sup>12</sup>, illustrated in Figure 5. Room temperature tensile properties of the final Ti-6Al-4V plate in the longitudinal direction included a yield stress,  $\sigma_y$ , of 930 MPa, and an ultimate tensile stress,  $\sigma_{UTS}$ , of 978 MPa<sup>3</sup>.

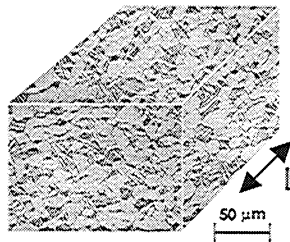


Figure 5: Microstructure of Ti-6Al-4V plate material<sup>3</sup>

## 2.2 Specimen & Ballistic Impact

Two diamond cross-section specimen geometries, typical of compressor airfoil leading edges, were machined to represent a “sharp” edge specimen and a “blunt” edge specimen, shown in Figure 6. The sharp specimens contained a 0.127 mm (0.005”) LE and the blunt specimens contained a 0.381 mm (0.015”) LE<sup>10</sup>.

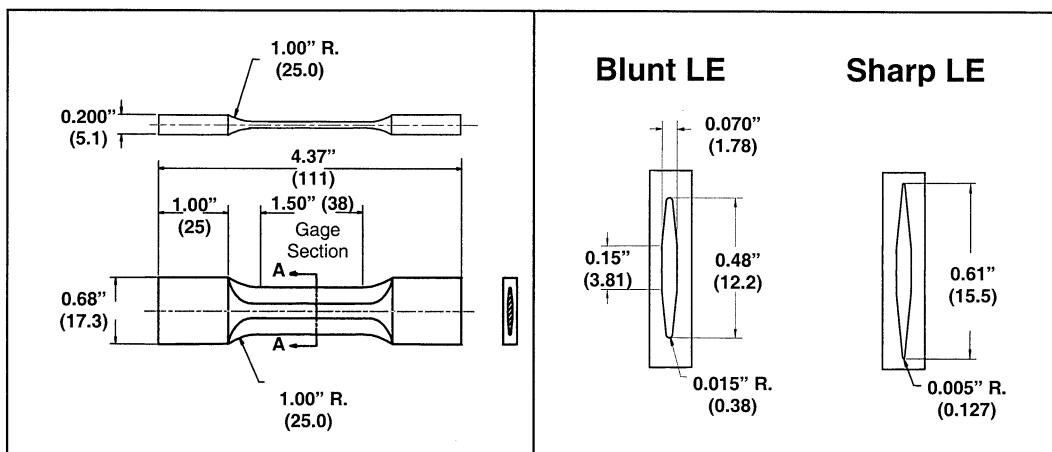


Figure 6: Diamond cross-section test specimen, dimensions in inches (mm).<sup>10</sup>

A single-stage compressed-gas gun was used to ballistically impact the samples. All impact tests were performed by the Impact Physics Group of the University of Dayton Research Institute. Figure 7 shows the schematic layout for ballistic impacting. Each specimen was impacted with 1 mm (0.040”) diameter glass beads to simulate sand and grit impacts experienced in the field. The incident angle of debris impacting the LE of in-service blades can vary from 10°

to  $60^\circ$  on the pressure side of the fan blade. Therefore, glass beads were shot at  $0^\circ$  or  $30^\circ$  incident angles, Figure 8a, to better represent fan and compressor blade FOD impacts<sup>11</sup>. The beads were shot at 305 m/s (1000 ft/s) which approximates the airflow of a foreign object relative to the blade during takeoff and landing, where most FOD occurs<sup>11</sup>. Samples were shot once on each leading edge on different planes, representing two potential crack initiation sites per sample. Both notches on a given sample, as shown in Figure 8b, had the same angle of incidence. Figure 9 is a series of high speed photographs of the ballistic impact of a 2 mm diameter glass bead<sup>12</sup>. The spheres typically shattered upon impact. These photographs were exposed at 100,000 frames per second, and the sequence begins from left to right.

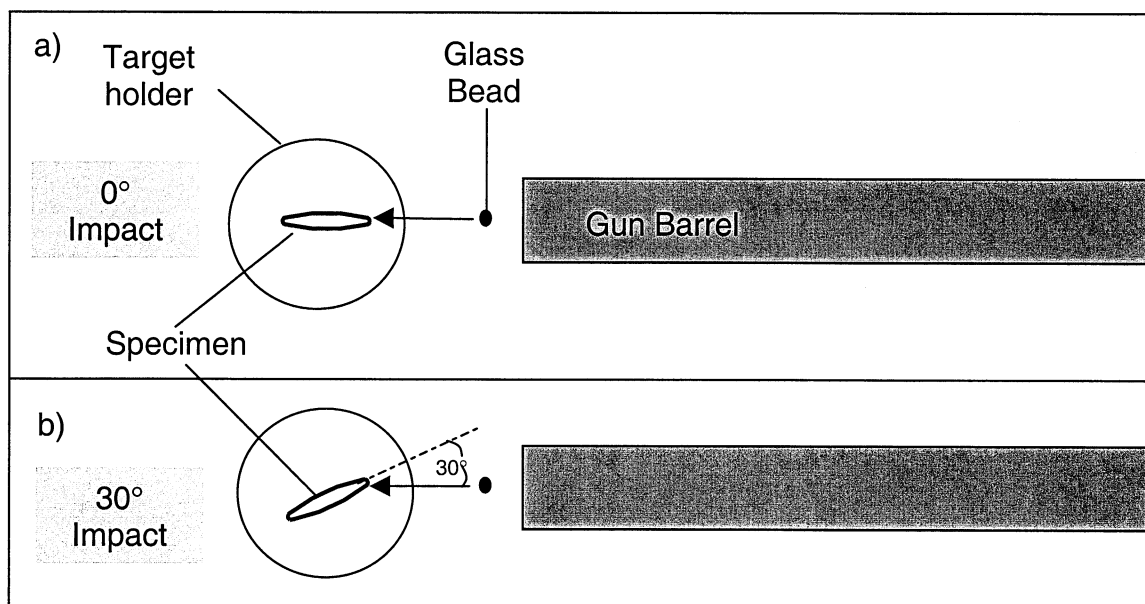


Figure 7: Schematic of ballistic impact

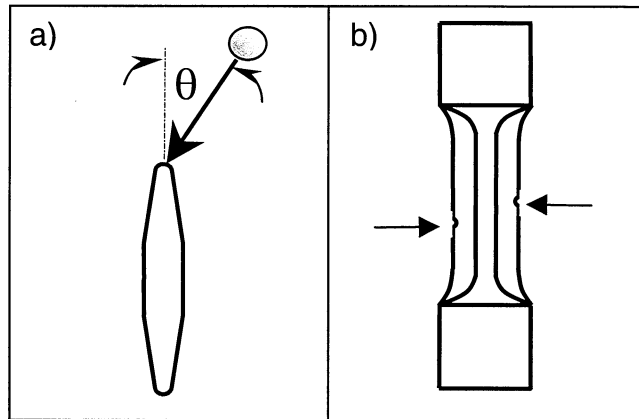


Figure 8: Ballistic Impact

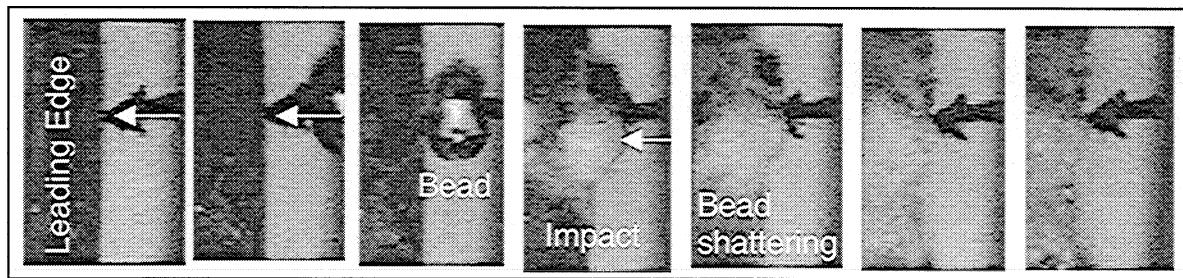


Figure 9: High speed film of 2 mm diameter glass bead impact<sup>12</sup>

### **2.3 Fatigue Testing**

Fatigue testing was performed by personnel at the U.S. Air Force Research Laboratory, Materials & Manufacturing Directorate. Since in-service blades undergo stress ratios ranging from  $R = 0.1$  to  $R = 0.8$ , two stress ratios of  $R = 0.1$  and  $0.5$  were chosen for this study to represent the idle and peak loading conditions for in-service blades<sup>1</sup>. Samples were subjected to tension-tension axial fatigue at 350 Hz.

$$R = \frac{\sigma_{\min}}{\sigma_{\max}}$$

Equation 1: Stress Ratio

A step loading procedure, which has been demonstrated to be effective on this material, was chosen<sup>7</sup>. Testing was performed under ambient temperature and humidity conditions. The samples were loaded at some initial stress and fatigued for  $10^7$  cycles. If the specimen did not fail, the load was increased by 10% of the initial load, and then fatigued for another  $10^7$  cycles. This process was repeated until the specimen failed at  $N_{\text{fail}}$ , shown in Figure 10, where  $N_{\text{fail}}$  is the number of cycles applied in the loading block where failure occurred. The fatigue strength was calculated by interpolation between the failure stress and the stress of the previous step shown in Equation 2<sup>10</sup>.

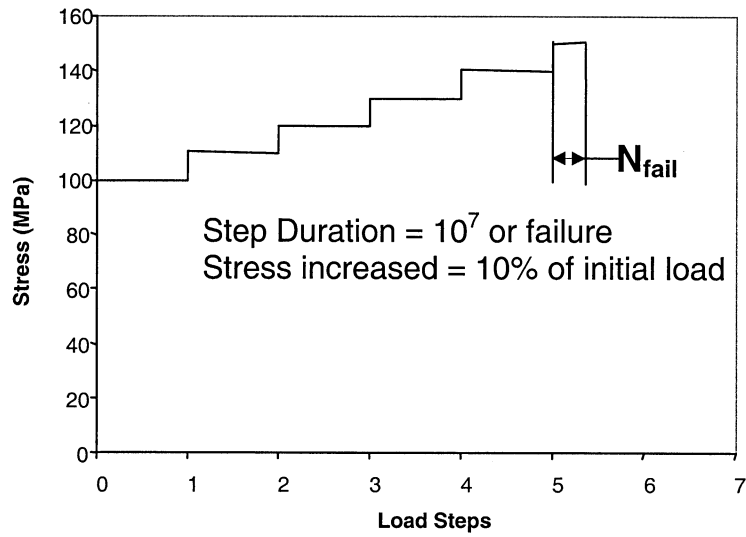


Figure 10: Fatigue step loading procedure<sup>12</sup>

Table 2: Strength Calculation Nomenclature

Nomenclature	Detail
$\sigma_e$	fatigue strength
$\sigma_o$	previous maximum failure stress (did not result in failure)
$\Delta\sigma$	step increase
$N_{block}$	$10^7$ cycles
$N_{fail}$	# of cycles in the loading block where failure occurred

$$\sigma_e = \sigma_o + \Delta\sigma \left( \frac{N_{fail}}{N_{block}} \right)$$

Equation 2: Fatigue Strength<sup>10</sup>

## **2.4 Notch Characterization**

Prior to fatigue testing, most samples were characterized by a scanning electron microscope (SEM) for initial FOD impact damage. The damage features characterized included the notch depth, material loss on the notch surface, material shear, material folding over the LE, embedded glass from the shattered bead, and microstructural damage such as deformed grains. These will be discussed later in further detail. The notches were photographed at a variety of views: normal to the leading edge (Figure 11a), in the direction of impact (Figure 11b), profile of the leading edge (Figure 11c), and profile of the notch (Figure 11d). Figure 12 shows the views taken for a failed notch at a 30° impact on a sharp LE. In addition, the broken samples were tilted 30° along the length of the LE to view the notch/fracture interface as seen in Figure 13. This view provided insight into the crack initiation location.

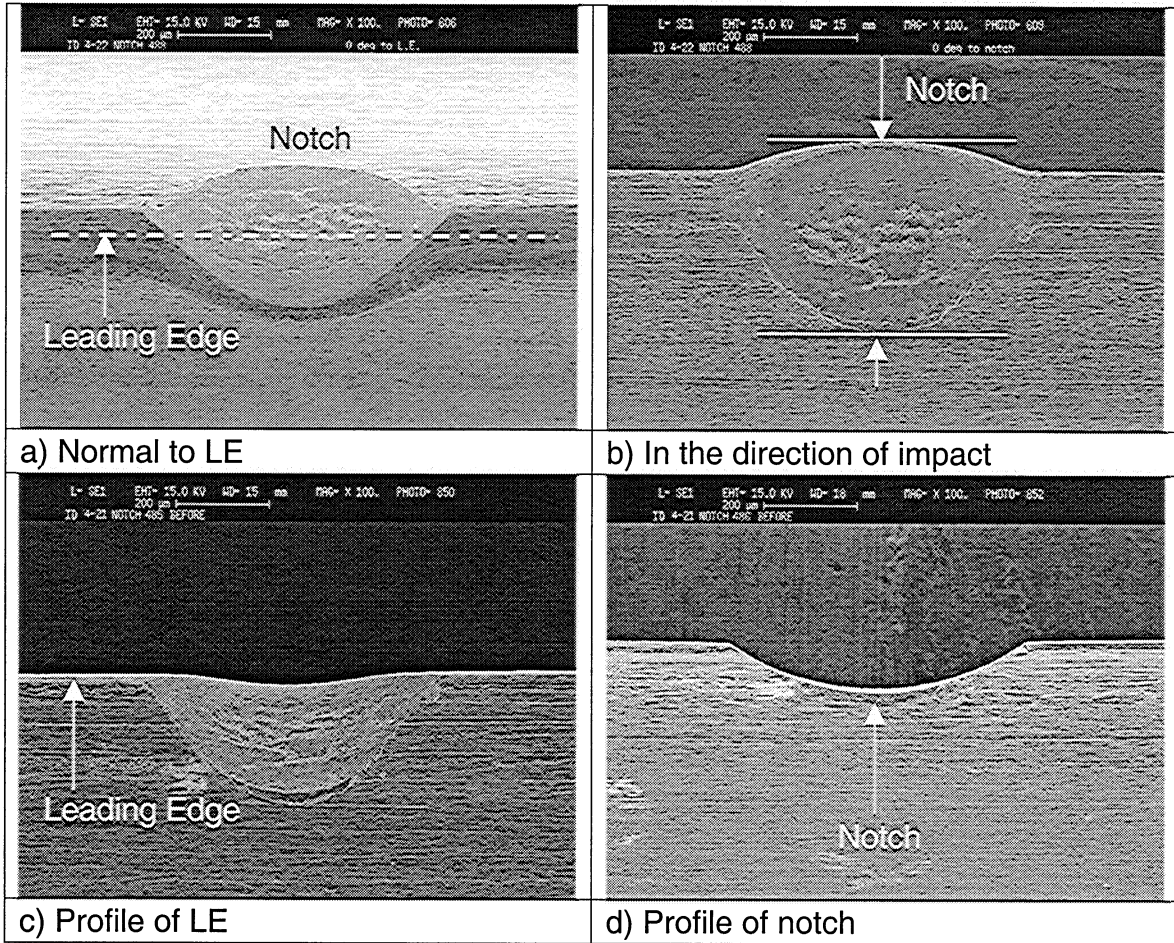


Figure 11: Un-failed notch for sample 4-22, with a sharp LE and a 30° impact



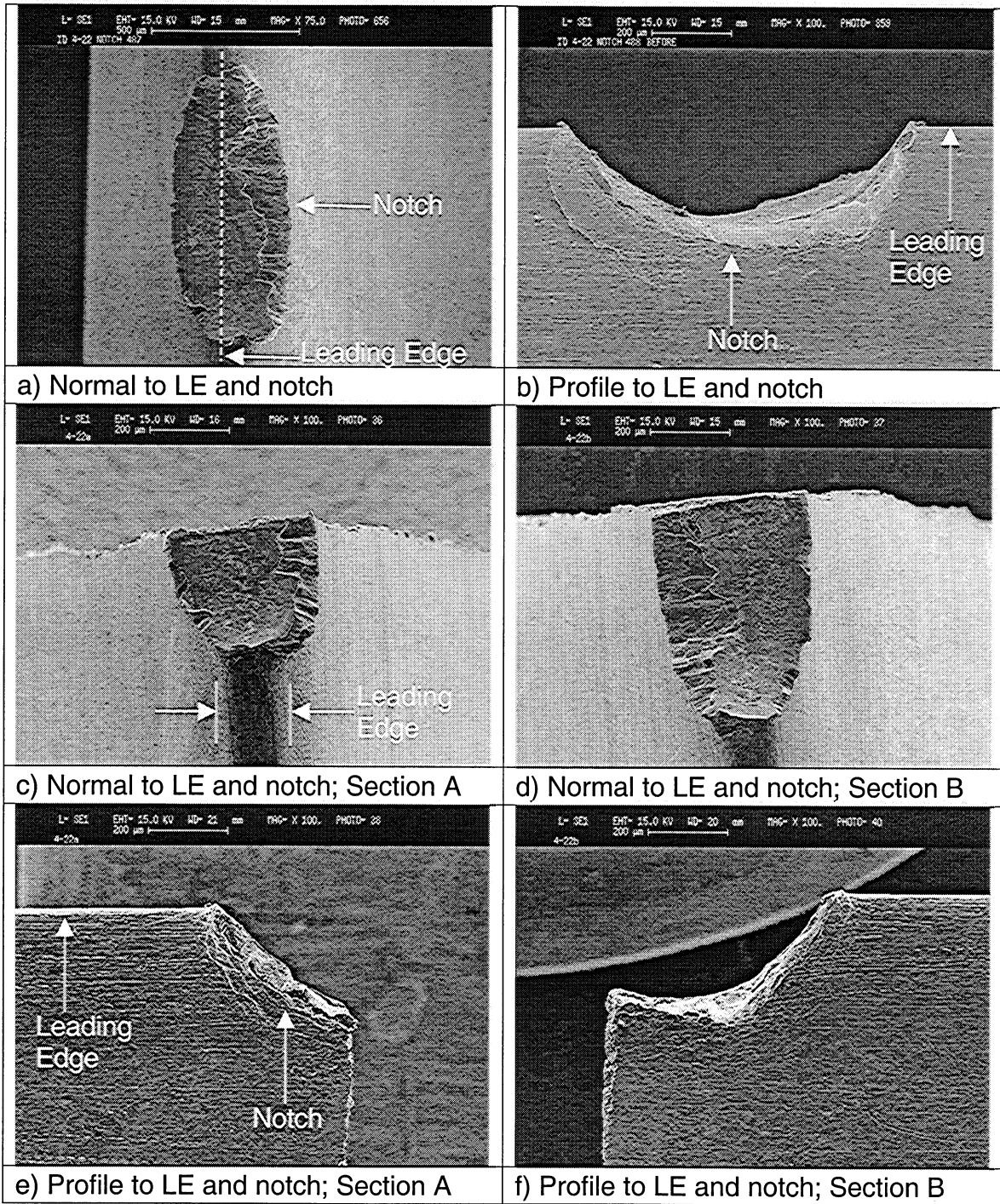


Figure 12: Failed notch for sample 4-22

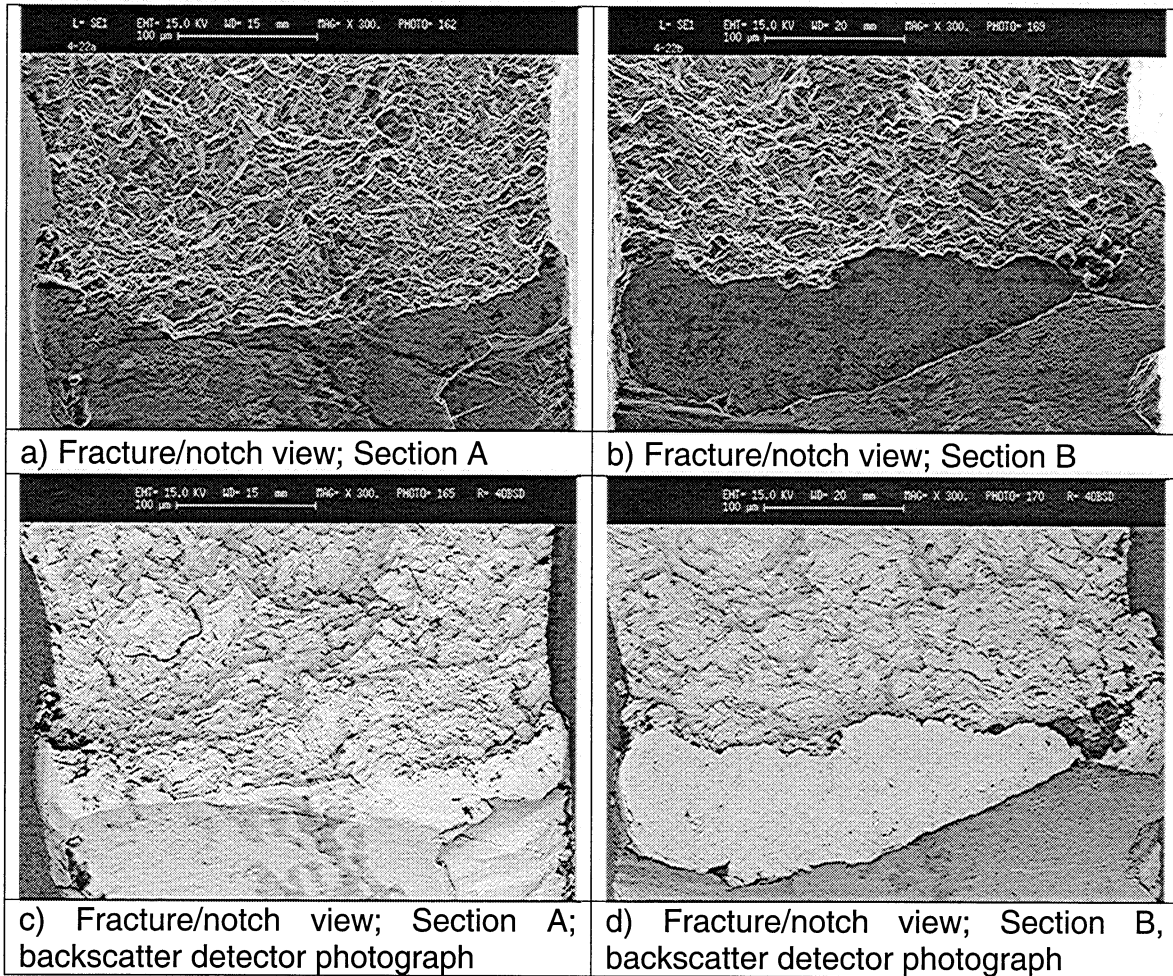


Figure 13: Fracture views of failed notch for sample 4-22

## **2.5 Sample polishing and micro-sectioning**

Selected fractured samples, Figure 14a, were mounted and micro-sectioned in order to inspect the damaged area near the fracture section. These samples were cut using a diamond saw ¼ inch down from the fracture surface and mounted, Figure 14b, using a conducting powder, and a Simplemet mounting press. The height of each mounted sample was measured and recorded. Then they were ground down 1.78 mm (.035") for the blunt LE and 1.0 mm (.039") for the sharp LE in order to reach the center of the LE, shown in Figure 15. The grinding process was achieved by using a Phoenix grinding/polishing machine. The sample was ground beginning with a 400 grit paper and then with a 600 grit paper.

Once the grinding process had been completed, the samples were polished beginning with a 15 µm diamond slurry followed with a 6 µm slurry on the same machine. For the final polishing, they were first placed in a 1 µm slurry on the Vibromet polisher overnight. Finally they were moved to a .05 µm slurry on the Mastermet polisher for 4 hours. All of the polishing was accomplished with diamond slurry.

The samples were etched using Kroll's etchant for Ti-6Al-4V (100ml of water, 4ml of nitric acid, and 2ml of Hf) after final polishing. The etchant was placed on the polished surface for approximately 30 seconds to 1 minute per

sample in order to bring out the microstructure. Photographs of the etched samples were taken using a microscope at a variety of magnifications: 50X, 100X, 200X, 500X, and 1000X.

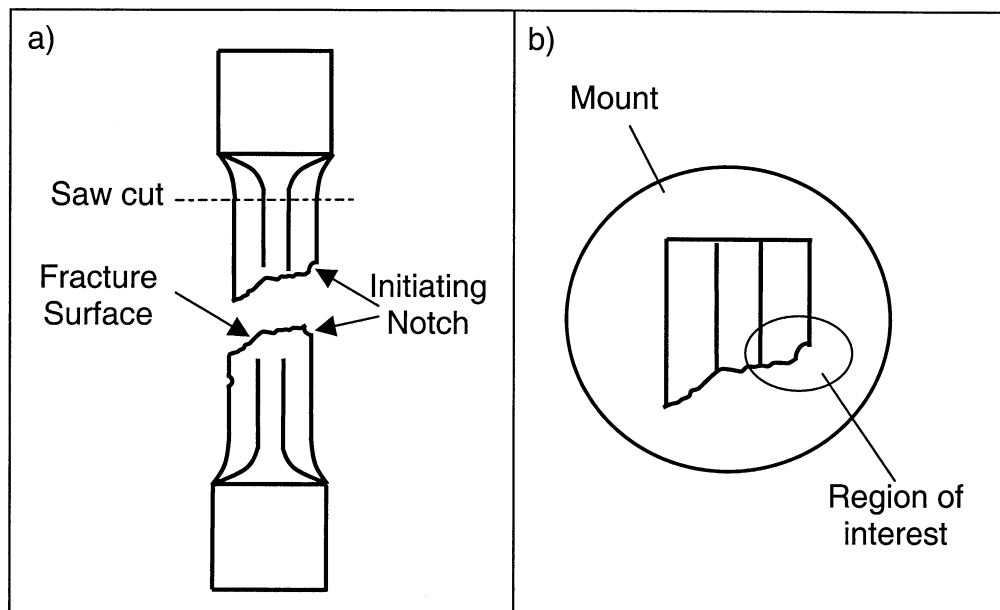


Figure 14: a) Illustration of Fractured Sample; b) Top view of mounted sample

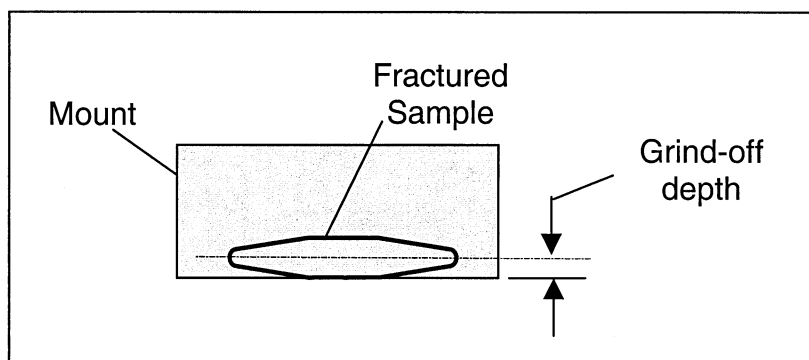


Figure 15: Profile view of mounted sample

### 3. RESULTS AND DISCUSSION

#### 3.1 Testing Conditions

The sample characterized consisted of a total of 34 specimens with two notches per sample. Both notches on each sample have the same angle of incidence. They were separated into 4 batches designated sample treatment, sample geometry, FOD, and fatigue test conditions. All of the untreated batches contained samples with both 0° and 30° shots, shown in Table 3. The heat-treated samples only contained 30° shots. These seven samples were stress relieved in order to evaluate the effect of residual stresses on the failure of the samples. They were heat-treated at 704°C (1300°F) for 1 hour in vacuum<sup>14</sup>.

Table 3: Samples characterized at the list of each condition

Batch	LE	Stress Ratio	Number of 0° samples	Number of 30° samples	Heat treated 30° samples
1	Sharp	0.1	2	6	2
2	Sharp	0.5	2	3	1
3	Blunt	0.1	2	4	2
4	Blunt	0.5	2	5	2

### 3.1.2 Effects of Angle of Incidence

Results of the tests performed on the samples for 0° and 30° incident angles are presented in Figure 16. The data represents the average normalized fatigue strength,  $\sigma_{norm}$ , for each batch at 0°, indicated by the clear bars, and at 30°, indicated by the shaded bars. The fatigue strength for each sample,  $\sigma_{sample}$ , was normalized using the fatigue strength of tested un-notched (un-impacted) smooth round-bar specimens,  $\sigma_{smooth}$  (Equation 3). The average fatigue strength of the smooth bar is 568 MPa at  $R = 0.1$  and 660 MPa at  $R = 0.5$ <sup>3</sup>. Normalized fatigue strength of 1.0 is that of the un-notched smooth bar sample, which is considered to have a 0% debit in fatigue strength. A reduction in fatigue strength would be indicated by an average normalized fatigue strength of less than 1.0, as seen in Figure 16.

$$\sigma_{norm} = \left( \frac{\sigma_{sample}}{\sigma_{smooth}} \right) \quad \text{Equation 3: Normalized Fatigue Strength}$$

All 34 impacted samples exhibited a decrease in fatigue strength. The 0° impacts appear to have lower fatigue strength degradation than the 30° impacts, see Figure 16. A surprising observation is that the sharp LE samples displayed higher fatigue strength than the blunt LE samples.

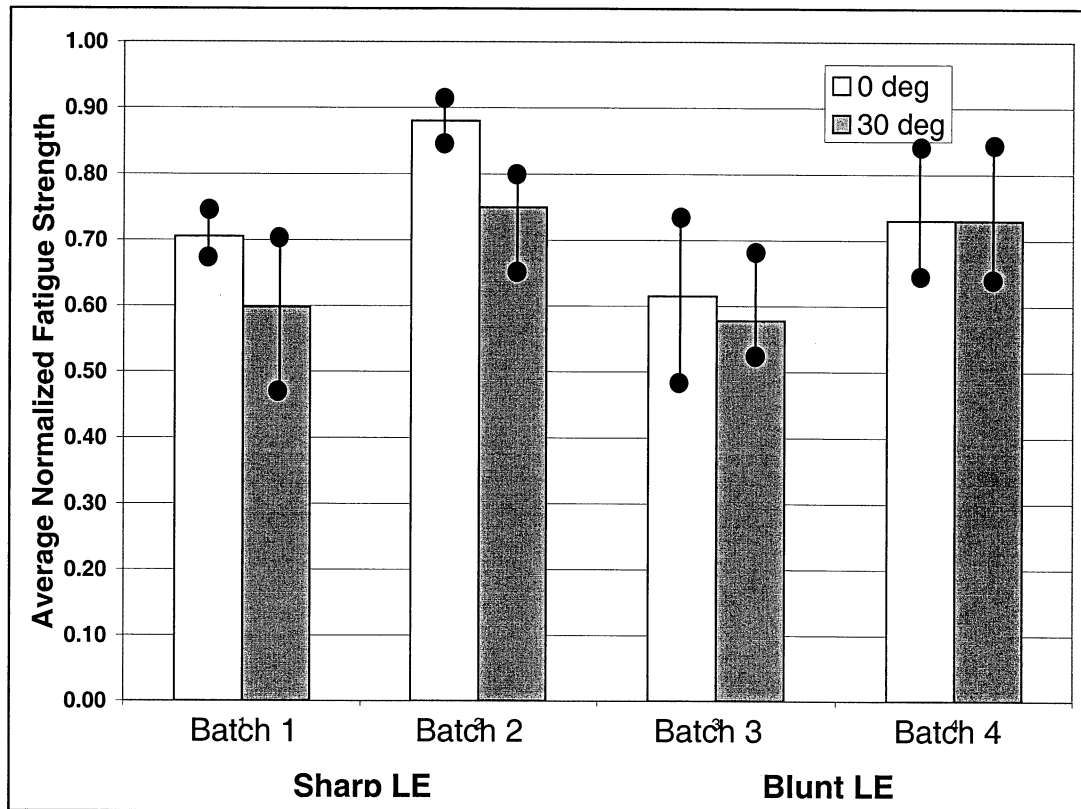


Figure 16: Average normalized fatigue strength of batches 1 through 4

Preliminary finite element analysis, conducted by C. Weeks<sup>14</sup>, implied that the impact of a 0° shot leaves behind residual compressive stresses on the notch area as shown in Figure 17a. If this is true, these compressive stresses, which are similar to those generated by shot peening, could result in an improvement of the fatigue strength at the notch area, see Figure 17a. Shot peening is a cold working process that results in residual compressive stresses which improves the fatigue strength of the component<sup>16</sup>.

It is hypothesized that the 30° impact samples, on the other hand, have a gradient of residual stresses across the notch area in the direction of impact<sup>14</sup>,

shown in Figure 17b. These stresses could range from tensile to compressive. The 30° impacts have an entrance and an exit in the notch area as the bead traveled through, leaving behind this gradient of residual stresses. True head-on 0° impacts do not, generally, have an entrance and an exit location; thus a gradient of tensile and compressive stresses would not exist.

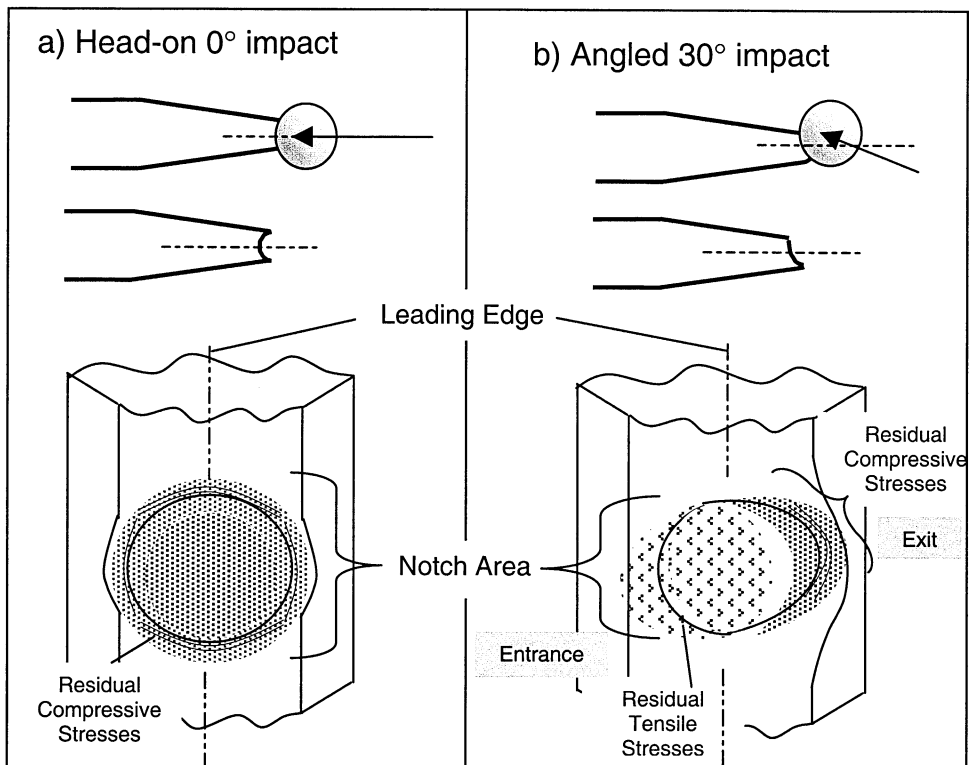


Figure 17: Schematic of residual stress fields on ballistic impact sites; a) A head-on 0° impact on a blunt LE; b) An angled impact on a blunt LE, the schematic is based on ref 14



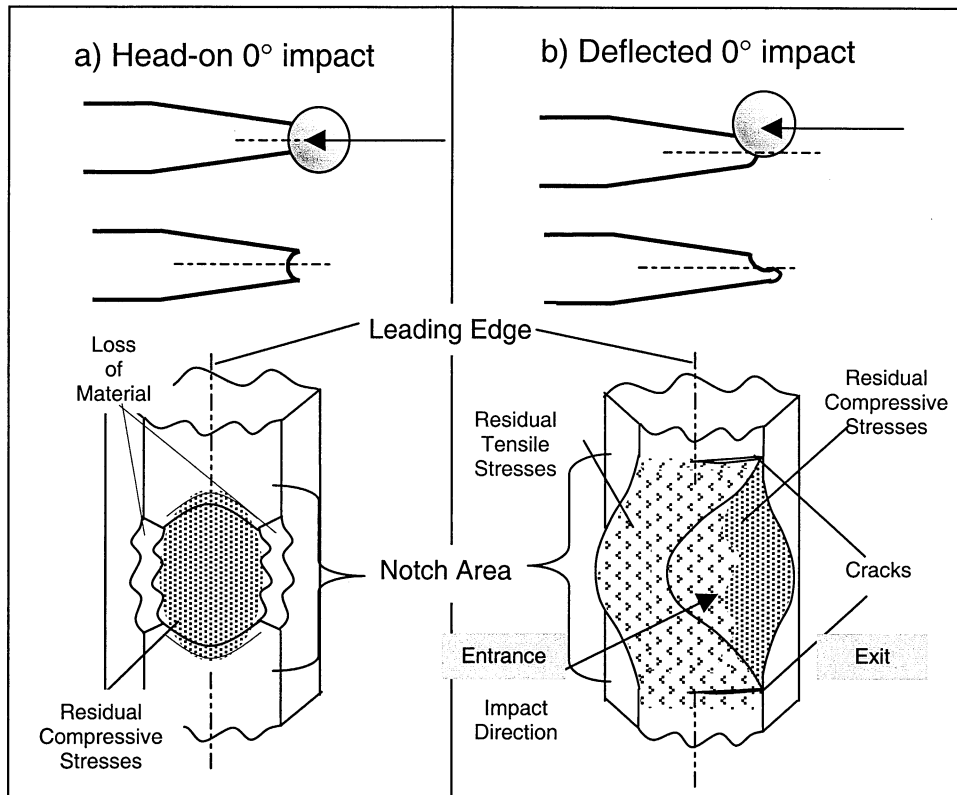


Figure 18: Postulated residual stress fields on ballistic impact sites; a) A head-on 0° impact on a sharp LE with loss of material; b) A deflected 0° compressing the sharp LE to one side. The schematic is based on ref 14

Approximately 80% of the 0° shots fired at the sharp LE samples did not hit the leading edge head on, but were off center as shown in Figure 18b. Figure 19 and Figure 20 show photographs of representative 0° impacts for both the sharp and the blunt edges. In each of those pictures the top photo shows the failed notch, and the bottom is that of the un-failed notch. The center of the LE is

indicated by the dashed line. The off center shots create little damage to the leading edge. Instead the material is shifted to one side, possibly leaving behind residual compressive and tensile stresses similar to that of an angled shot shown in Figure 17b and Figure 18b. As expected, the sharp edge is difficult to hit head on. Consequently, none of the  $0^\circ$  impacts hit the LE head-on, instead they impacted on one side of the LE, compressing it as suggested in Figure 19. This may be one reason why the  $0^\circ$  impact samples showed higher fatigue strength than the  $30^\circ$  impact samples, especially for the sharp edge samples. In this case, there might be a higher level of residual compressive stresses than a typical angled impact, because the bead compresses the material to one side instead of shearing it from entrance to exit.

Since the blunt LE is wider, 25% of the  $0^\circ$  impacts actually hit the LE head-on, with the remaining 75% resembling those of angled or  $30^\circ$  impacts on blunt edges, shown in Figure 20. These  $0^\circ$  impacts produced more damage on the blunt edge than those for the sharp edge. The similarity in fatigue strength debit between the  $0^\circ$  and  $30^\circ$  impacts for the blunt LE could be due to the fact that the damage from  $0^\circ$  impacts resemble that of damage from  $30^\circ$  impacts.

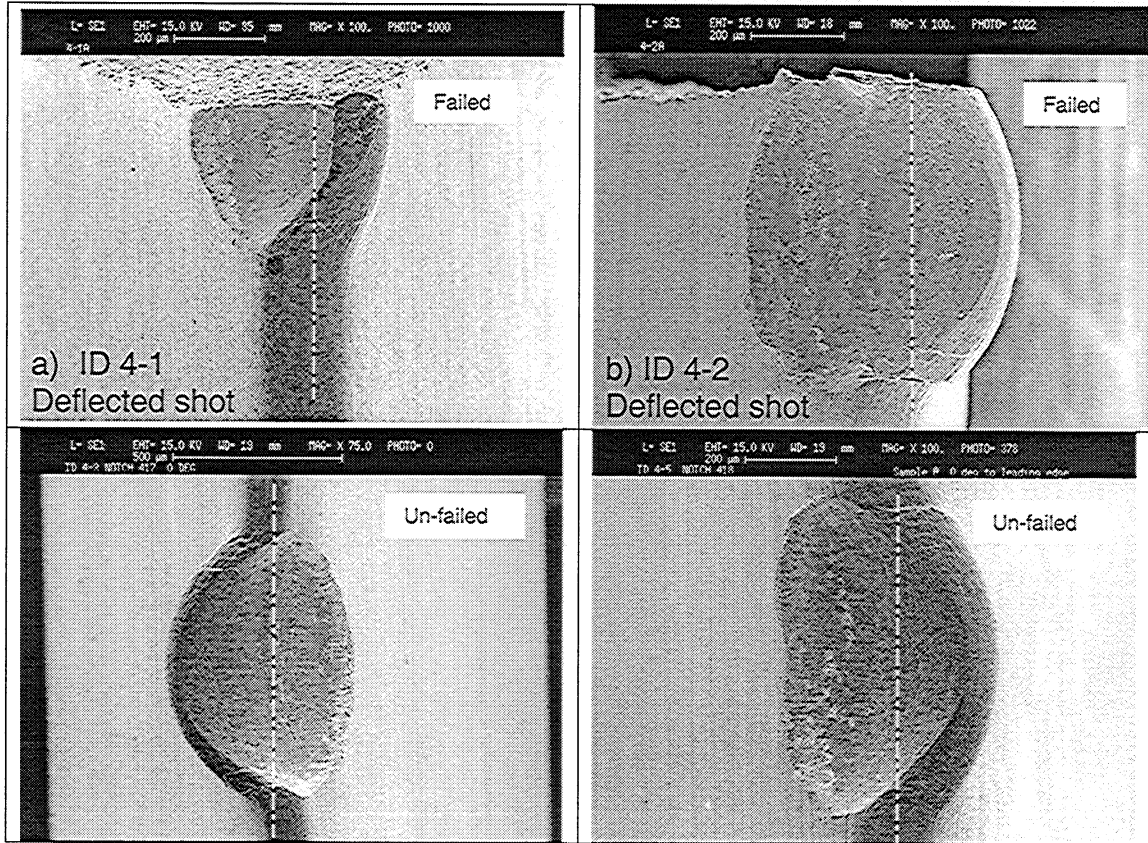


Figure 19: Sharp LE with 0° impacts showing both failed and un-failed notches.

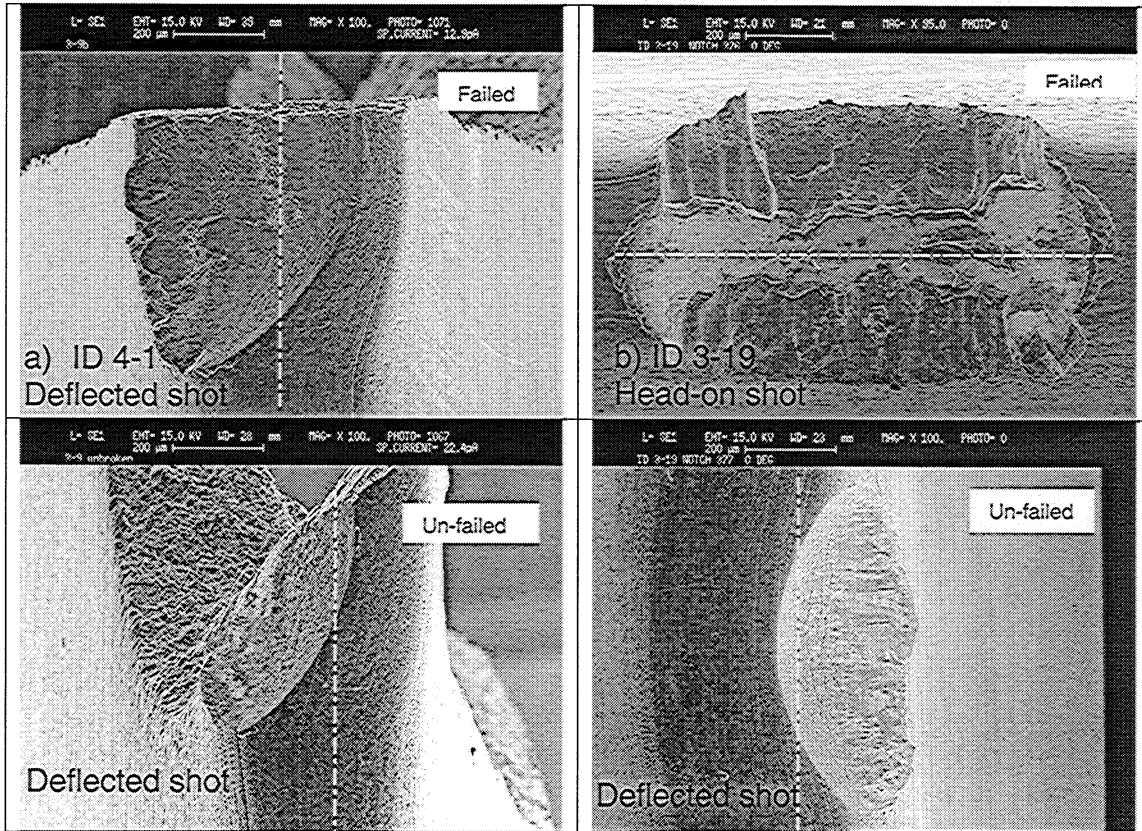


Figure 20: Blunt LE with 0° impacts showing both failed and un-failed notches.

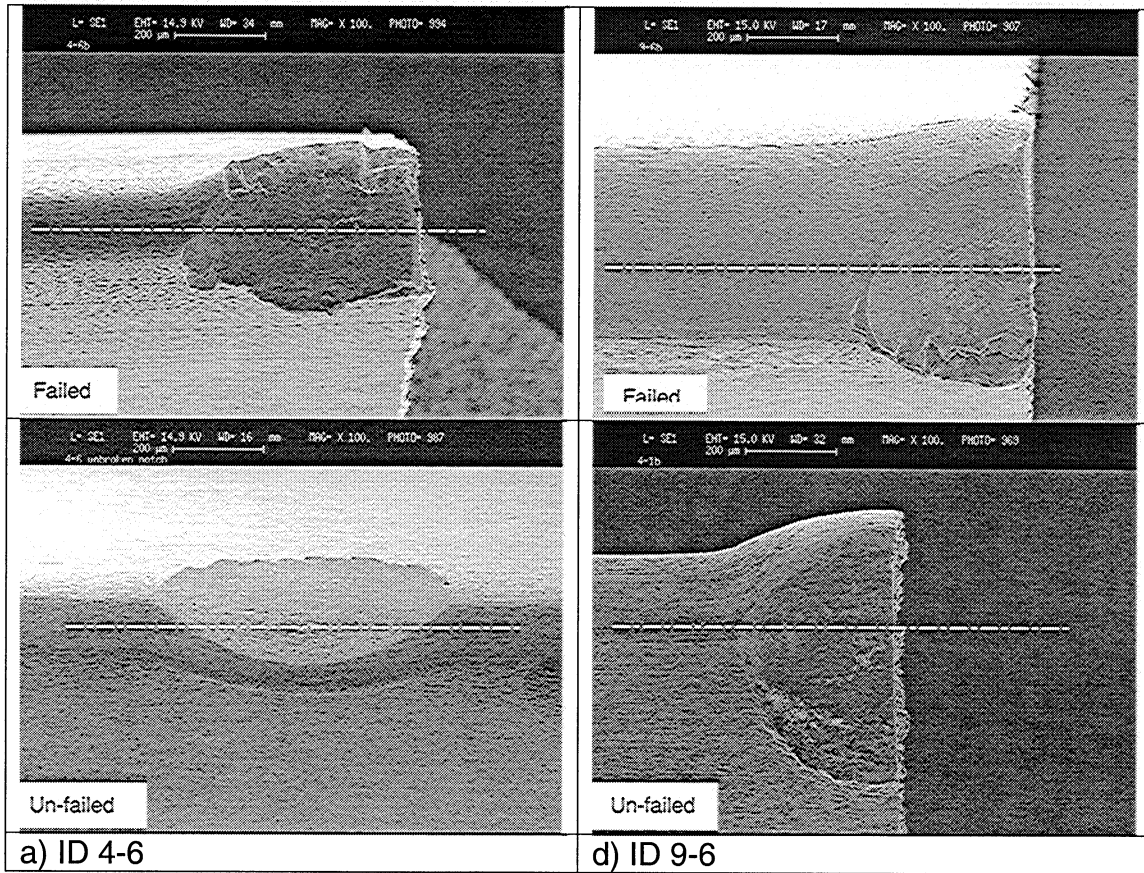


Figure 21: Samples with 30° impacts showing both failed and un-failed notches.

a) Sharp LE; b) Blunt LE

### ***3.1.3 Effects of Leading Edge Radius***

Even though the sharp edge was difficult to hit head-on, most of the 30° impacts did not miss. Figure 22 illustrates the effect of LE radius on the normalized fatigue strength for both incident angles. The data is sufficiently scattered to conclude that the LE radius has little or no effect on the fatigue strength of FOD impacted samples. Further data on the effects of edge radius on fatigue strength can be found in Figure 23 for both incident angles. Here the estimated loss of material is compared to the fatigue strength for sharp and blunt LE. Again, there is no clear correlation between the two. LOM will be discussed later.

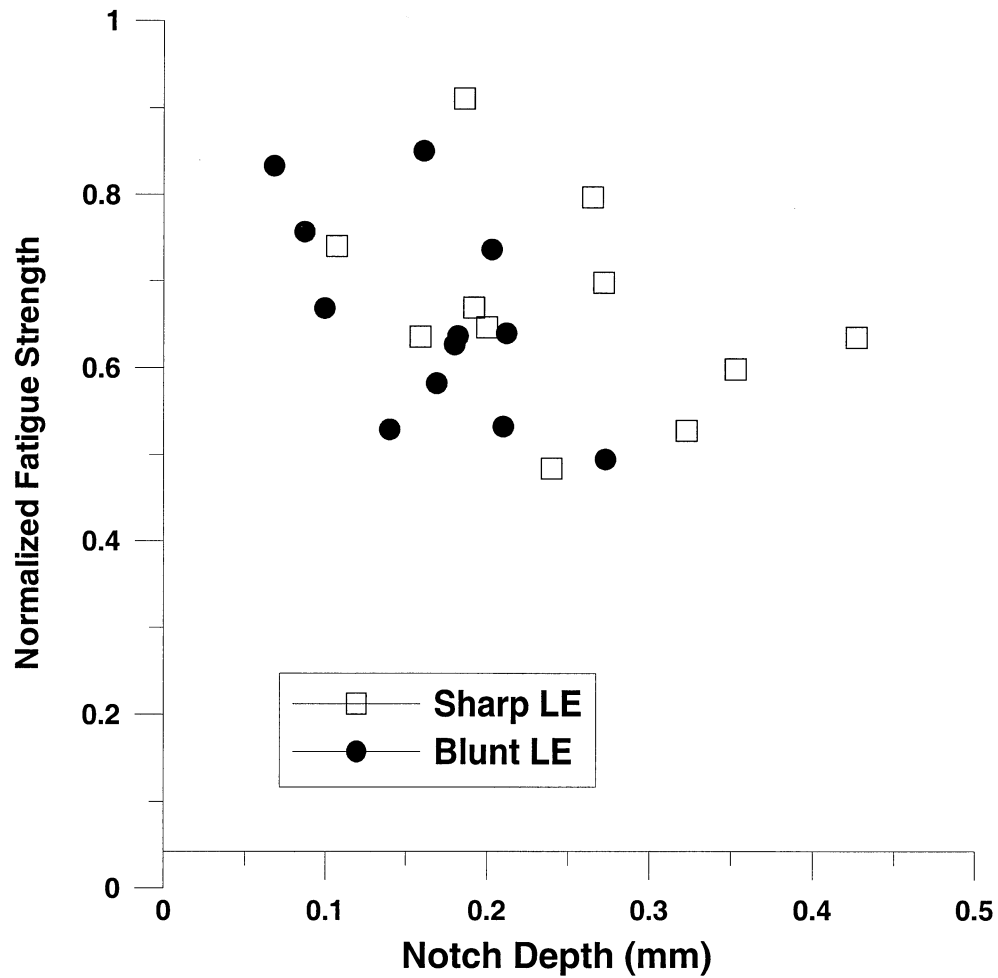


Figure 22: Notch depth vs. normalized fatigue strength for sharp and blunt LE and for both 0° and 30° impacts.

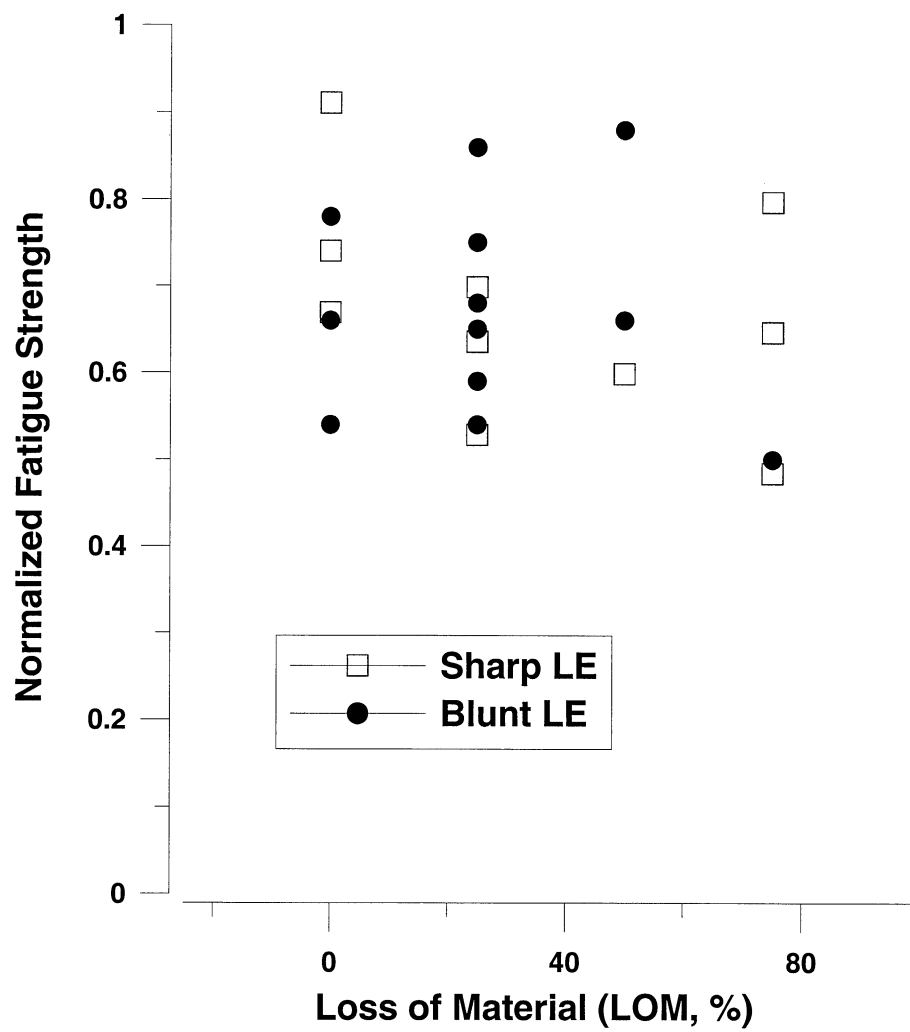


Figure 23: Loss of Material vs. normalized fatigue strength for sharp and blunt LE and for both 0° and 30° impacts.



### ***3.1.4 Effects of Heat Treatment***

Seven samples were stress relieved to study the effects of residual stresses on the fatigue strength debit of impacted samples. The annealing process was conducted at 704°C (1300°F) for 1 hour in vacuum<sup>14</sup>. A comparison of the results for the four testing conditions is summarized in Figure 24. The average normalized fatigue strength of un-stress relieved samples is compared to stress relieved samples, see Table 4. The stress relieved samples generally showed higher fatigue strength over the non-stress relieved except for batch 2. Unfortunately there was only one sample (9-1) tested for batch 2 shown in Figure 25. This sample showed severe damage with large amounts of material loss, embedded glass (indicated by the dark areas in Figure 25c), and jagged edges providing suitable crack initiation sites, shown in Figure 25b. Figure 26 shows one of the notches for each of the remaining stress relieved samples tested. Two of the seven samples did not fail at either notch, shown in Figure 26d and f. Both damage sites on each of those samples were very similar. Figure 26d shows that the bead did not impact the center of the LE but dented it from the side. On the other hand, in Figure 26f the bead hit head on to the LE and provided a good impact site. For both of these two samples, there was not much damage in the form of material loss, folds and embedded glass. The annealing process reduced any residual tensile and compressive stresses that would have

been present, which, as discussed in previous sections, may be beneficial or detrimental to fatigue strength. In contrast, the remaining five samples exhibited damage sites with loss of material, shown in Figure 26a, c and e. Figure 26b does not have loss of material, but it does contain embedded glass. Most of the samples, which failed at one of the two notches, contained embedded glass. It is possible that some silicon from the glass diffused during annealing into the titanium alloy producing an embrittled area in the notch<sup>19</sup>, thus providing a weak spot in the notch area, susceptible to failure. The loss of compressive or tensile residual stresses appear to play a role in the level of fatigue strength degradation. However, damage on the impact zone seems to play a more significant role in fatigue strength degradation.

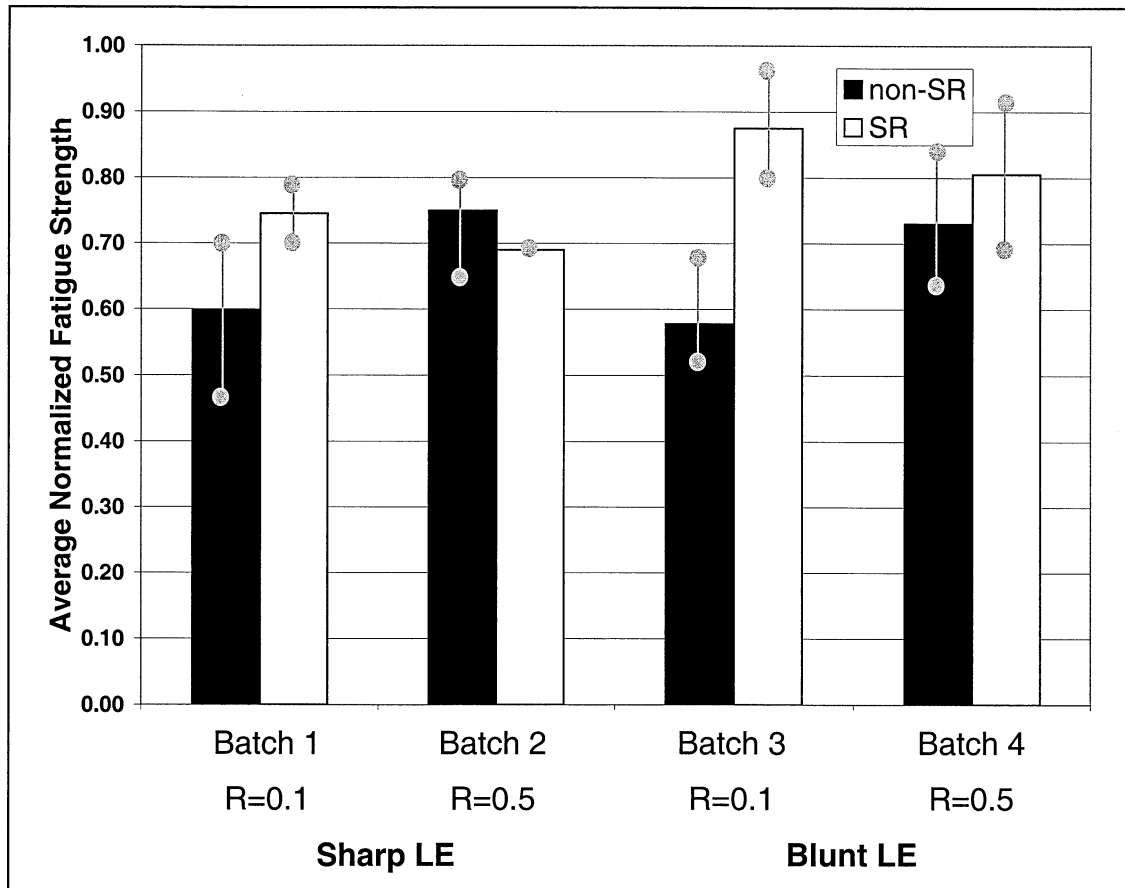


Figure 24: Average Normalized Fatigue strength for all testing conditions for 30° impacts.

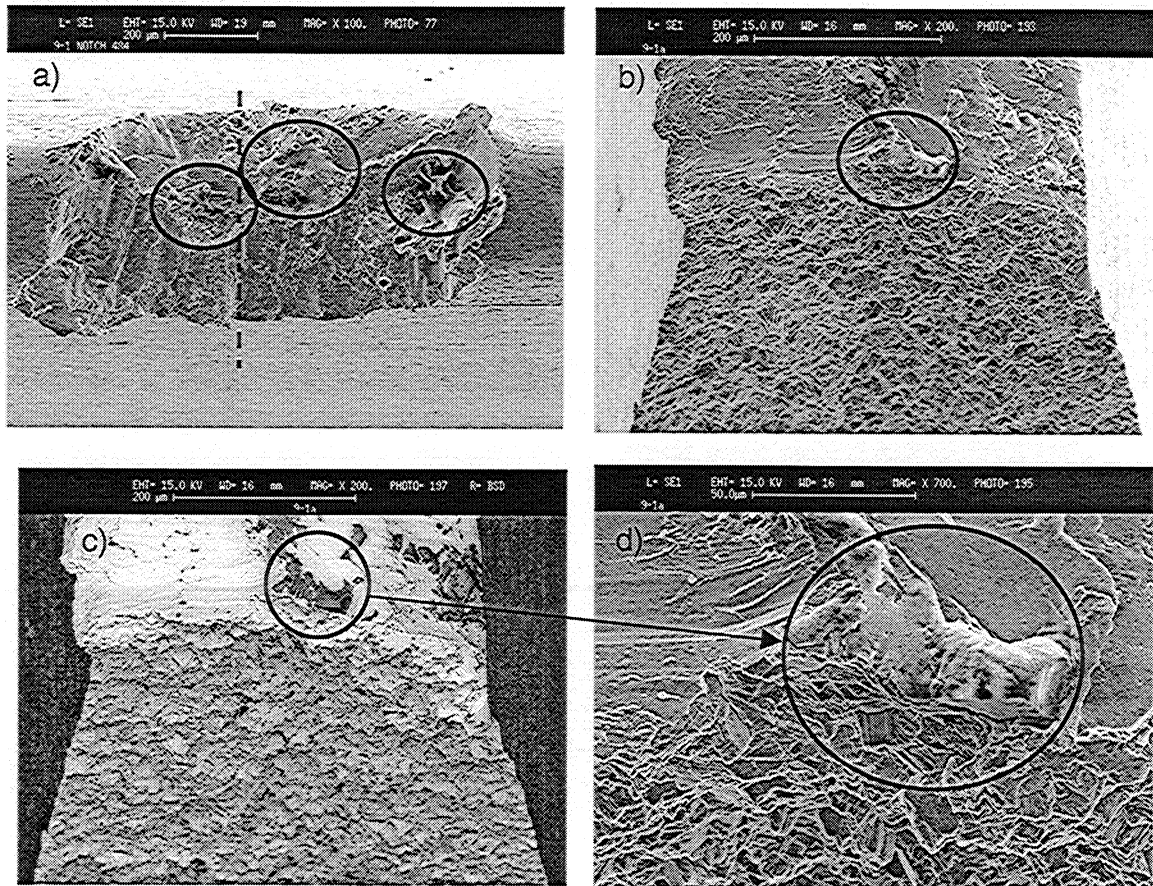


Figure 25: Sample 9-1, 30° impact; a) pre-fracture photo, b) post-fracture, c) backscatter detector image of b, d) close-up of b and c. Embedded glass is indicated by the circle,.

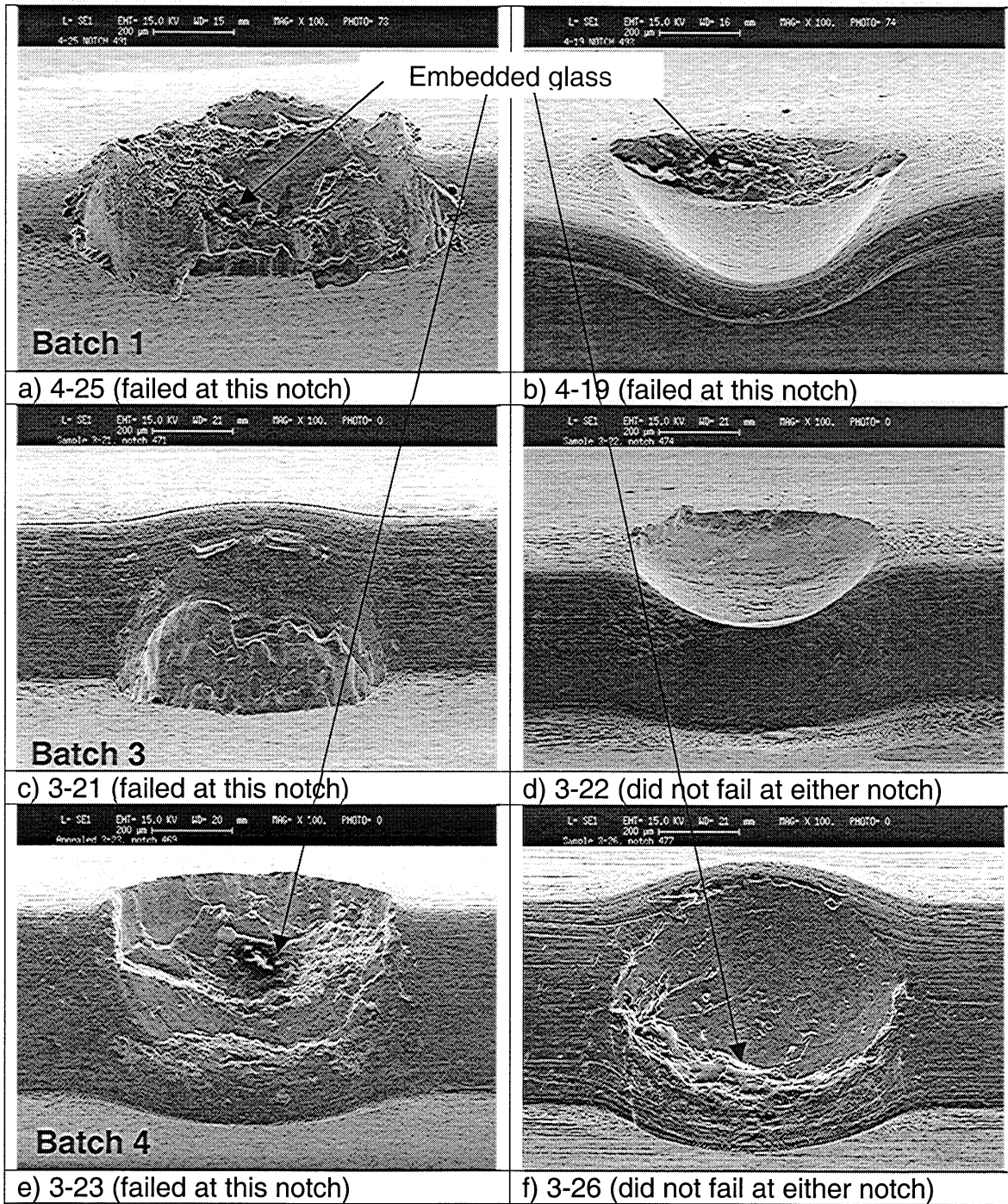


Figure 26: Stress relieved samples

### **3.2 Effects of Damage Features**

The damage features being characterized are the result of ballistic impact. These include the notch depth, loss of material on the notch surface (LOM), microstructural damage such as deformed grains, and other damage features such as material shear, material folding over the LE, and embedded glass from the shattered bead.

#### ***3.2.1 Effects of Notch Depth***

The notch depth was measured by rotating the SEM stage to achieve a profile view of the notch, as shown in Figure 27. These two notches are from the same sample and were impacted at 30°. Figure 27a shows a fairly shallow notch with loss of material and Figure 27b shows a deeper notch with loss of material. Figure 28 is a comparison of the depth of the failed notch, where crack initiation occurred, and the un-failed notch for each specimen impacted at 0°. In most of the cases, where failure initiated at the notch, it failed at the deeper of the two notches. The average damage depth of failed notches is 0.2 mm (0.008”) and 0.12 mm (0.005”) for un-failed notches. The 0° impacts failed at the deeper notch 65% of the time. The 30° impacts failed at the deeper of the two 85% of the time, as shown in Figure 29. Figure 30 shows that the failed notch alone had no direct effect on the normalized fatigue strength.

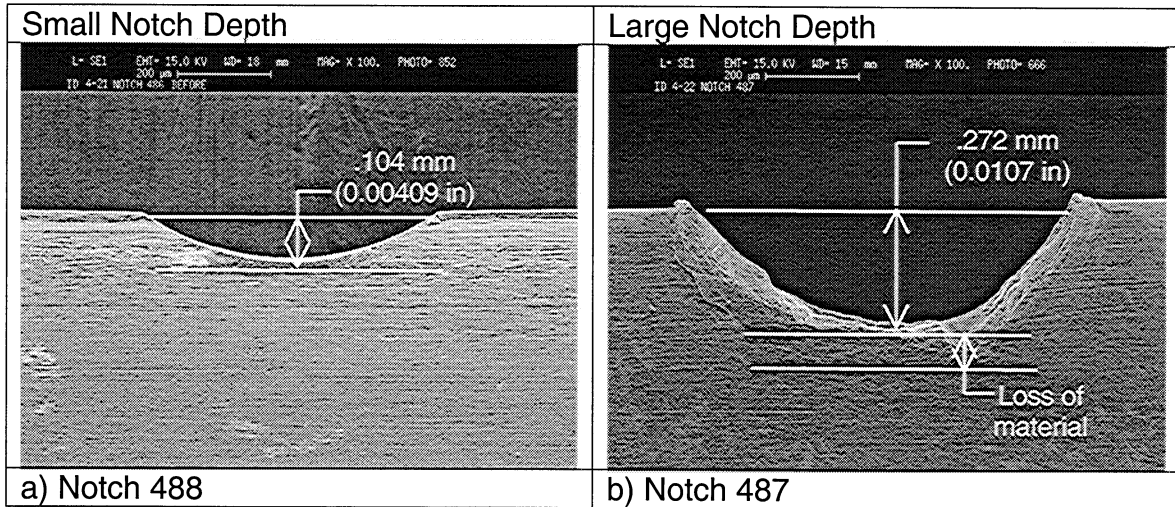


Figure 27: Characteristic Notch Depth (sharp LE with a 30° impact, sample 4-22)

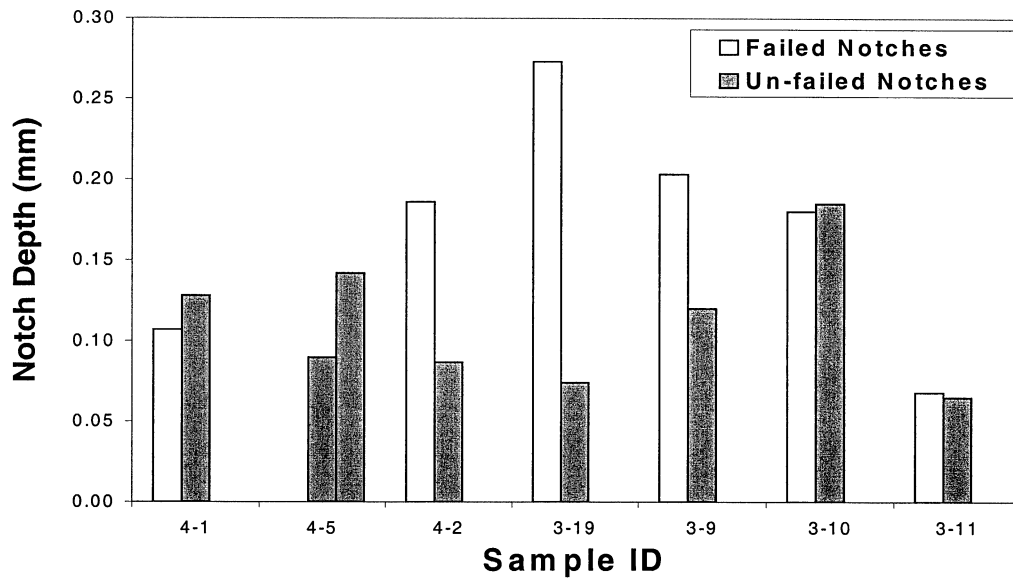


Figure 28: Depth of failed vs. un-failed notches for 0° impacts (sharp and blunt LE).

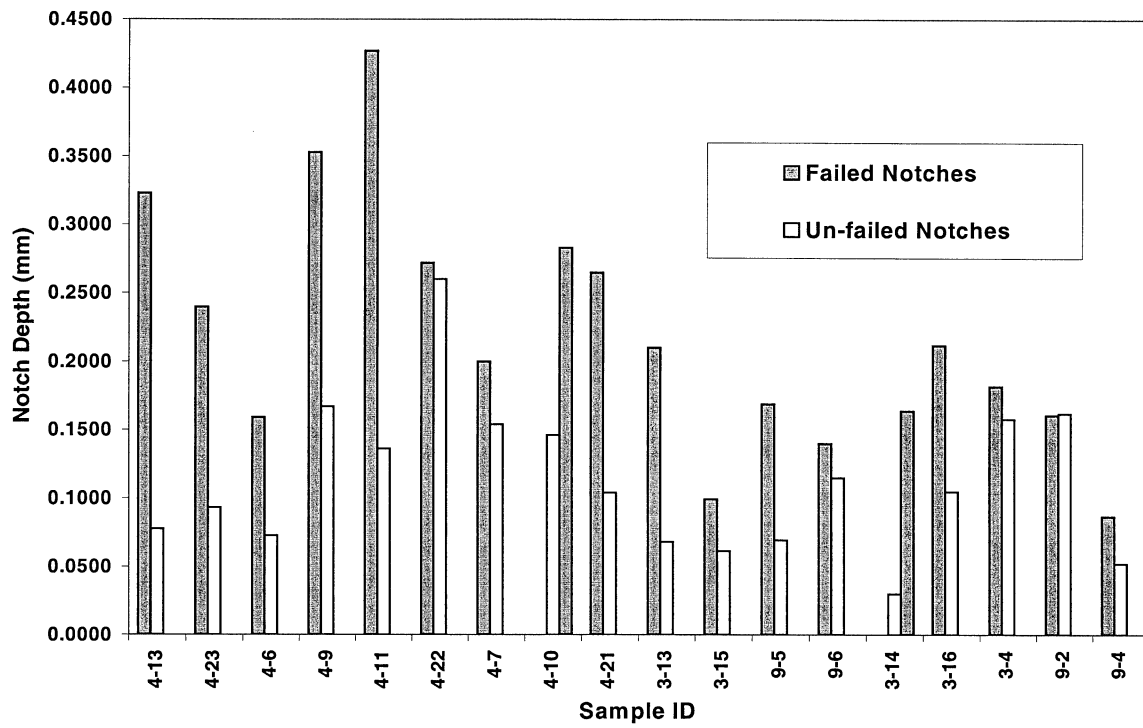


Figure 29: Depth of failed vs. un-failed notches for 30° impacts (sharp and blunt LE)



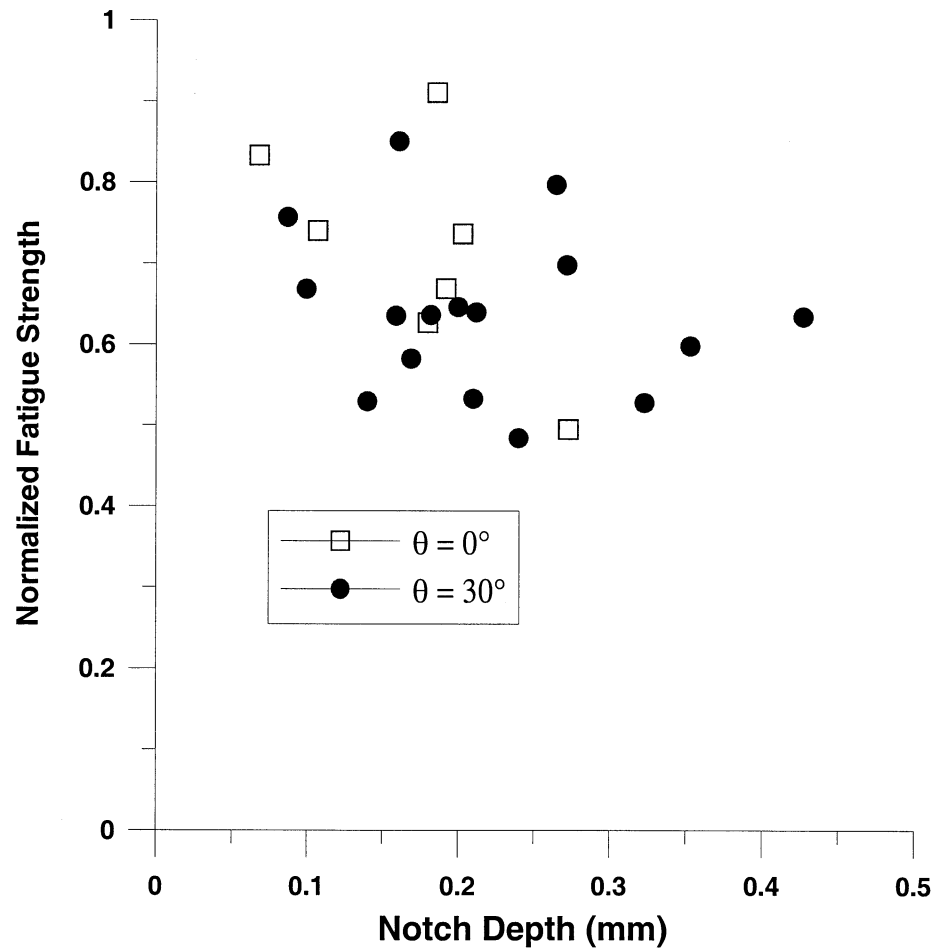


Figure 30: Notch depth vs normalized fatigue strength (sharp and blunt LE)

### ***3.2.2 Effects of Loss of Material (LOM)***

Another feature observed was the loss of material (LOM) from the surface of the notch, which was found on 65% of the failed notches and only 20% of the unfailed notches. This feature was observed and characterized, as shown in Figure 31, by visual estimation using an SEM, where the two notches are from the same sample. Figure 31a illustrates a notch with no material loss and a smooth surface. This is a 30° impact, where the bead seems to have only “dented” the leading edge. On the other hand, Figure 31b shows a rough and jagged notch where there is material loss. Crack initiation occurred at this notch.

In Figure 32, an attempt was made to correlate the loss of material for the failed notches to the average normalized fatigue strength. Loss of material for 30° impacts shows highly scattered results indicating that LOM alone has no clear effect on fatigue strength. However, there is a general trend to the average normalized fatigue strength for the 0° impacts such that the larger the material loss, the lower the fatigue strength. Unfortunately, only two out of eight 0° impacts actually hit head-on to the LE, Figure 32 b and c, the remaining six missed the edge slightly and created an abnormal impact, seen in Figure 32a. Additional 0° impacted samples need to be tested to confirm this trend due to the fact that the high cycle fatigue strengths are so highly scattered. Even though

the amount of LOM may not have an effect on fatigue strength debit, the result of such damage can produce sharp edges and micro-folds on the surface of the notch or the possibility that as material is removed, so are the residual compressive stresses in that area. Samples generally failed at the notch with LOM: 81% of the 30° impacted samples failed at the notch with LOM, shown in Figure 33, and 75% for the 0° impacted samples, shown in Figure 34.

In most cases LOM provides a suitable crack initiation site for failure to occur. Figure 35 illustrates the fracture surface for sample 3-19 (shown in Figure 32c), with a large amount of LOM. In addition to the LOM, the notch contained embedded glass from the shattered bead. The crack did not initiate at the embedded glass, but at a slight fold in the LOM section of the notch denoted by the circle. The depth of this notch was 0.273 mm (0.0107") and the fatigue strength debit of this sample was 49% of an un-notched sample.

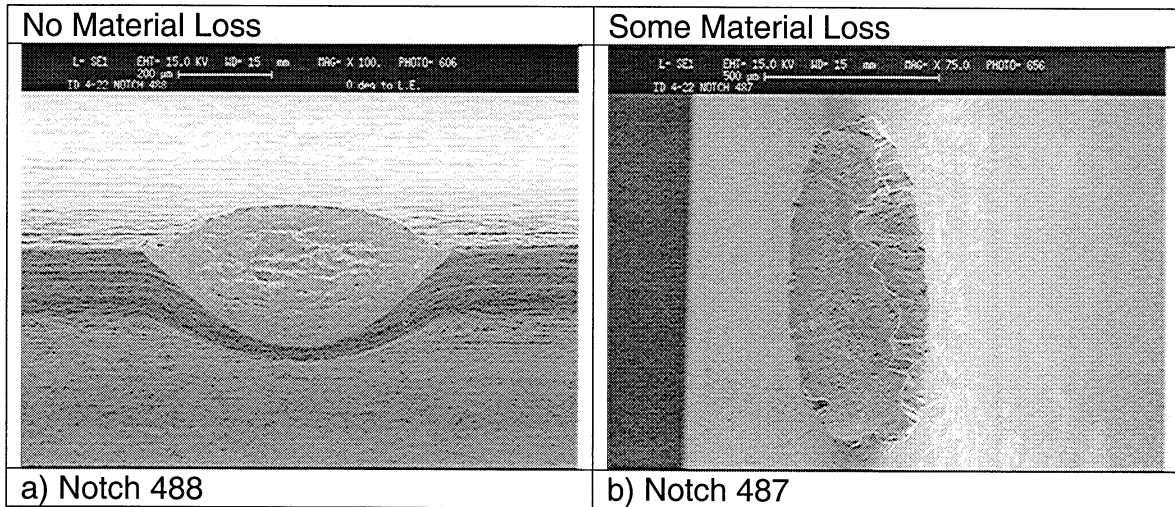


Figure 31: Loss of Material (sharp LE with a 30° impact, sample 4-22)

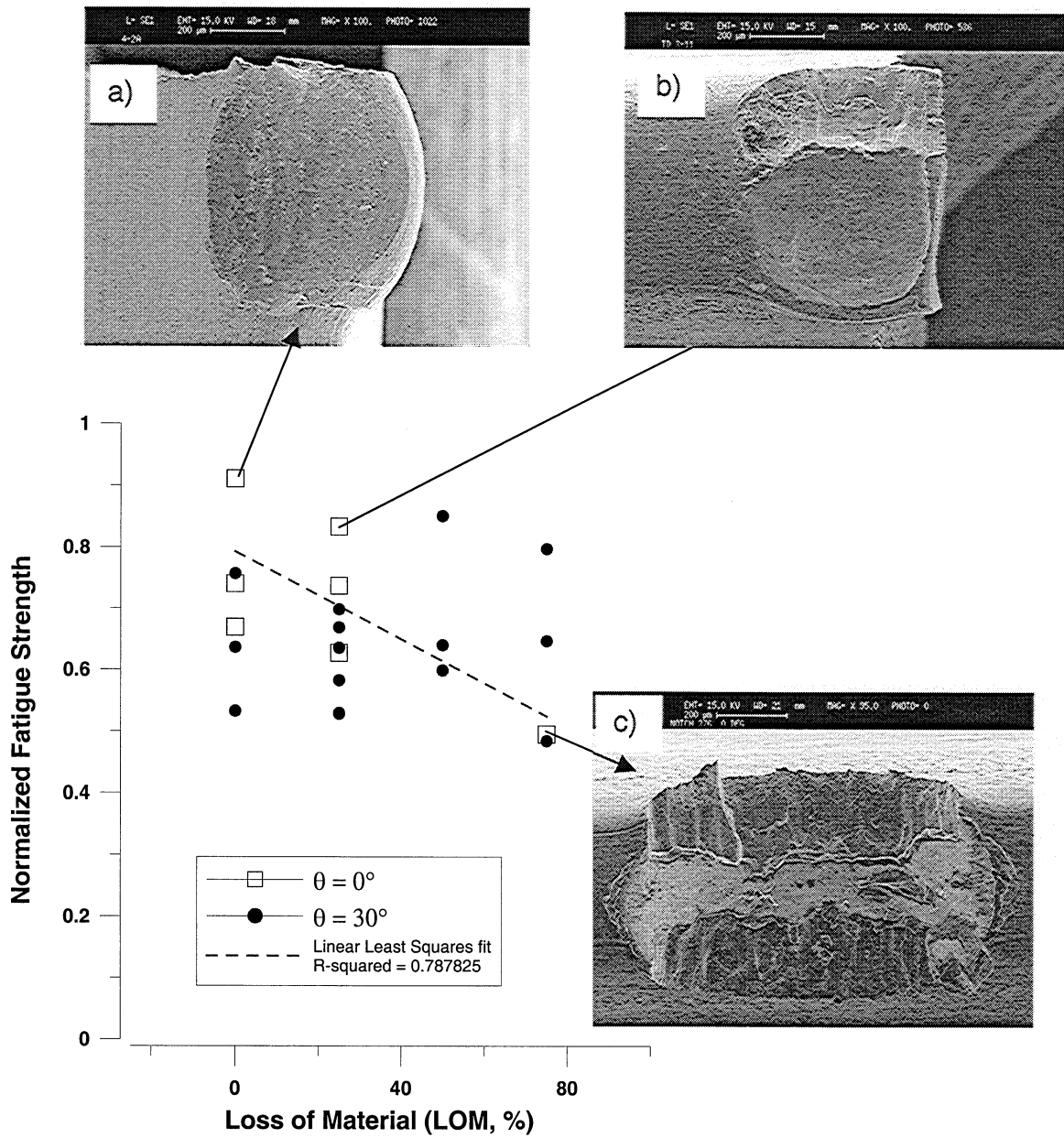


Figure 32: Comparison of materials loss and the fatigue strength; linear squares fit for  $0^\circ$  impacts. (sharp and blunt LE)

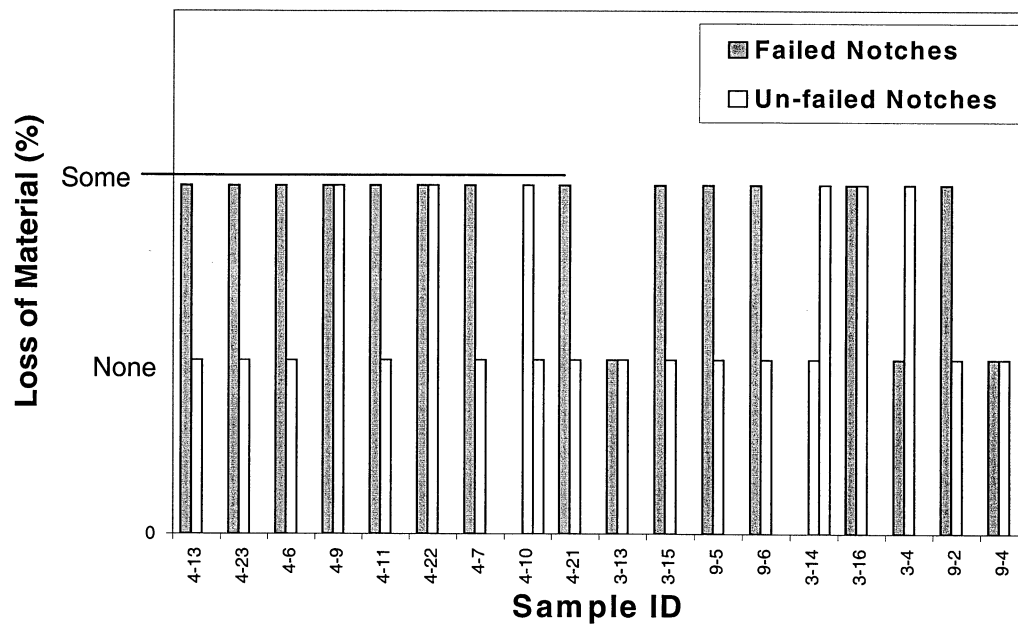


Figure 33: LOM for failed vs. un-failed notches for 30° impacts (sharp and blunt LE)

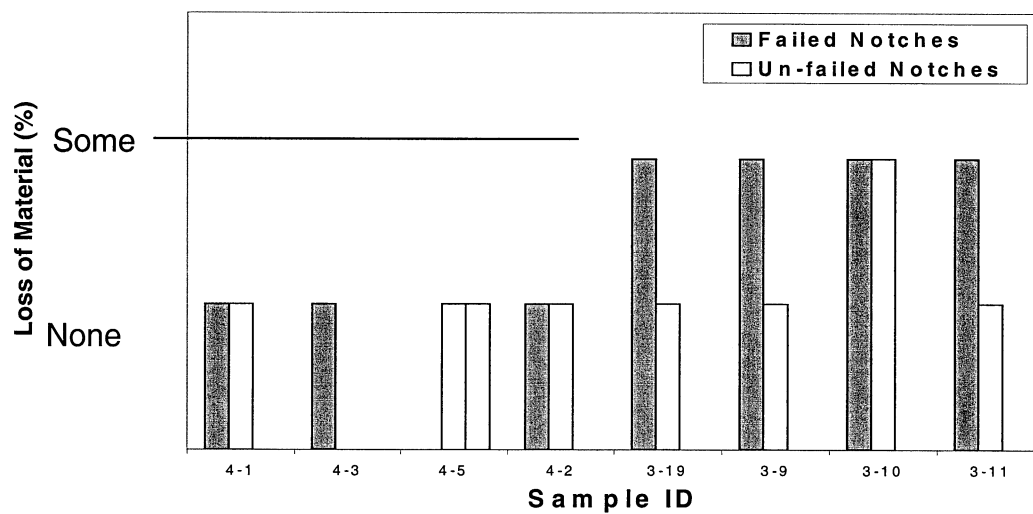


Figure 34: LOM for failed vs. un-failed notches for 0° impacts (sharp and blunt LE)

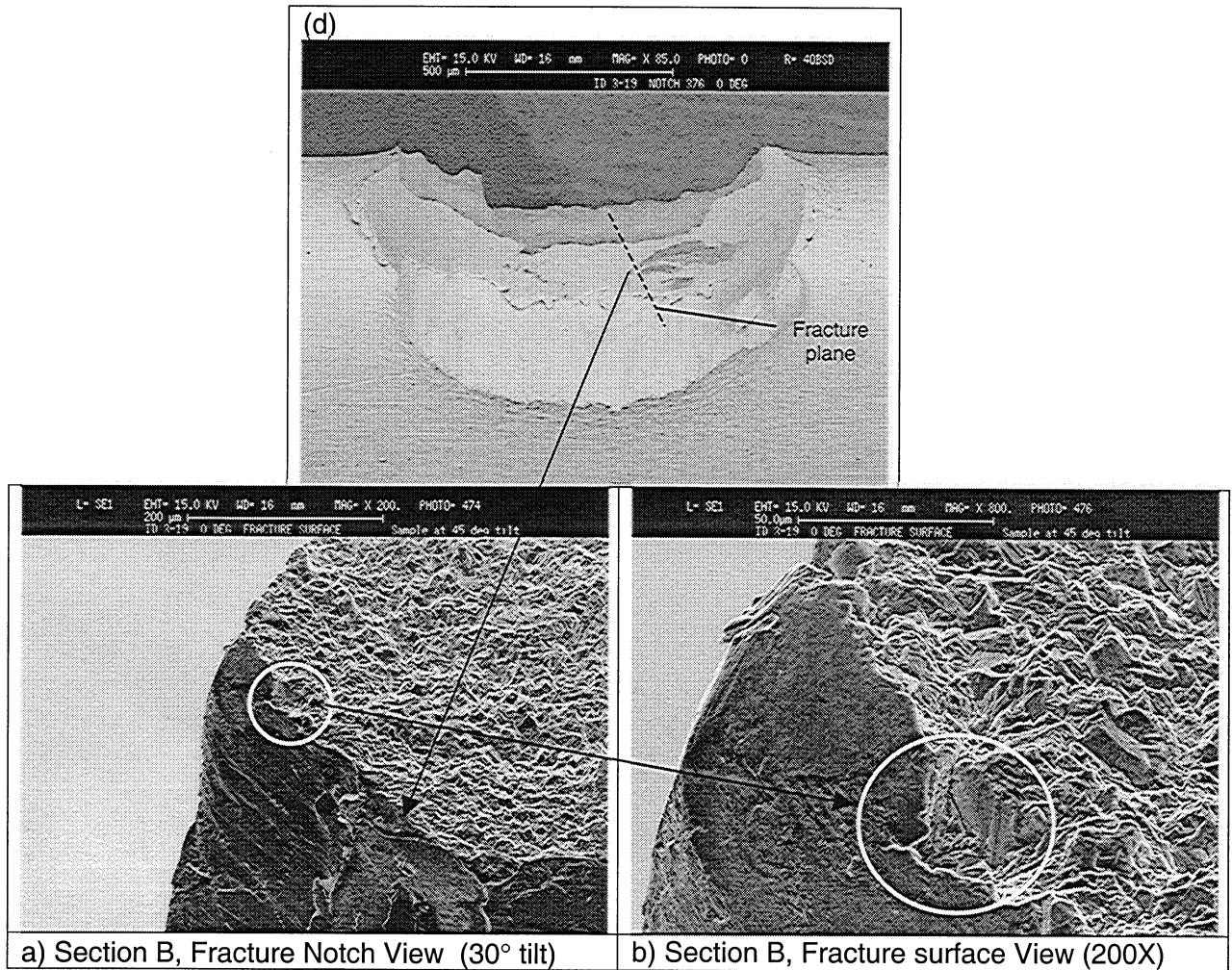


Figure 35: Fracture initiation of Sample 3-19 (blunt LE with a 0° impact)

### 3.2.3 Effects of Microstructural Damage

Precision micro-sectioning was performed on a limited number of fatigued samples. An example is shown in Figure 36. These particular photos were taken at the mid-plane of a fractured sample with a 53% fatigue strength debit and a notch depth of 0.21-mm (0.0083"). Evident from each photo is a band of deformed grains along the periphery of the notch, typically 60-100  $\mu\text{m}$  wide. While there was no evidence of subsurface cracking in the direction of eventual crack growth in any of the samples examined, multiple shear bands roughly parallel to the notch were observed in all of the micro-sectioned samples. The fact that these bands are oriented parallel to the applied loading direction (perpendicular to eventual fatigue cracking and to the impact direction) indicates that their presence may have little influence on the fatigue life.

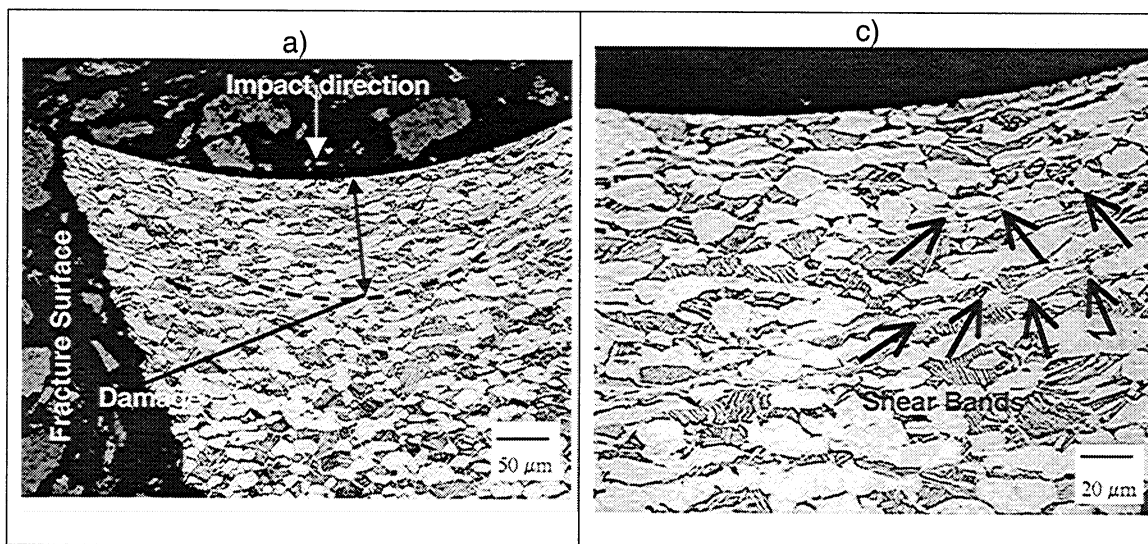


Figure 36: Precision Micro-sectioning of sample 3-13



### ***3.2.4 Effects of Other Features***

Other damage features that were apparent in the impacts include material shear in the notch region (Figure 37a & b), material folding over the LE (Figure 37c), and embedded glass from the shattered bead (Figure 37d) which was confirmed by energy dispersive spectroscopy, shown in Appendix B. None of these features alone appeared to have any significant effect on the fatigue strength. On the other hand, shearing and folds did provide suitable crack initiation sites for some of the samples. Figure 38 illustrates the fracture of sample 3-4, which had a notch depth of 0.182-mm (0.0071") and a fatigue strength debit of 64%. The pre-fracture condition of the notch indicates a material shear (or tearing) indicated by the circle in Figure 38a. The post-fracture condition of the notch shows that the fracture initiated somewhere behind the material shear, Figure 38b & c.

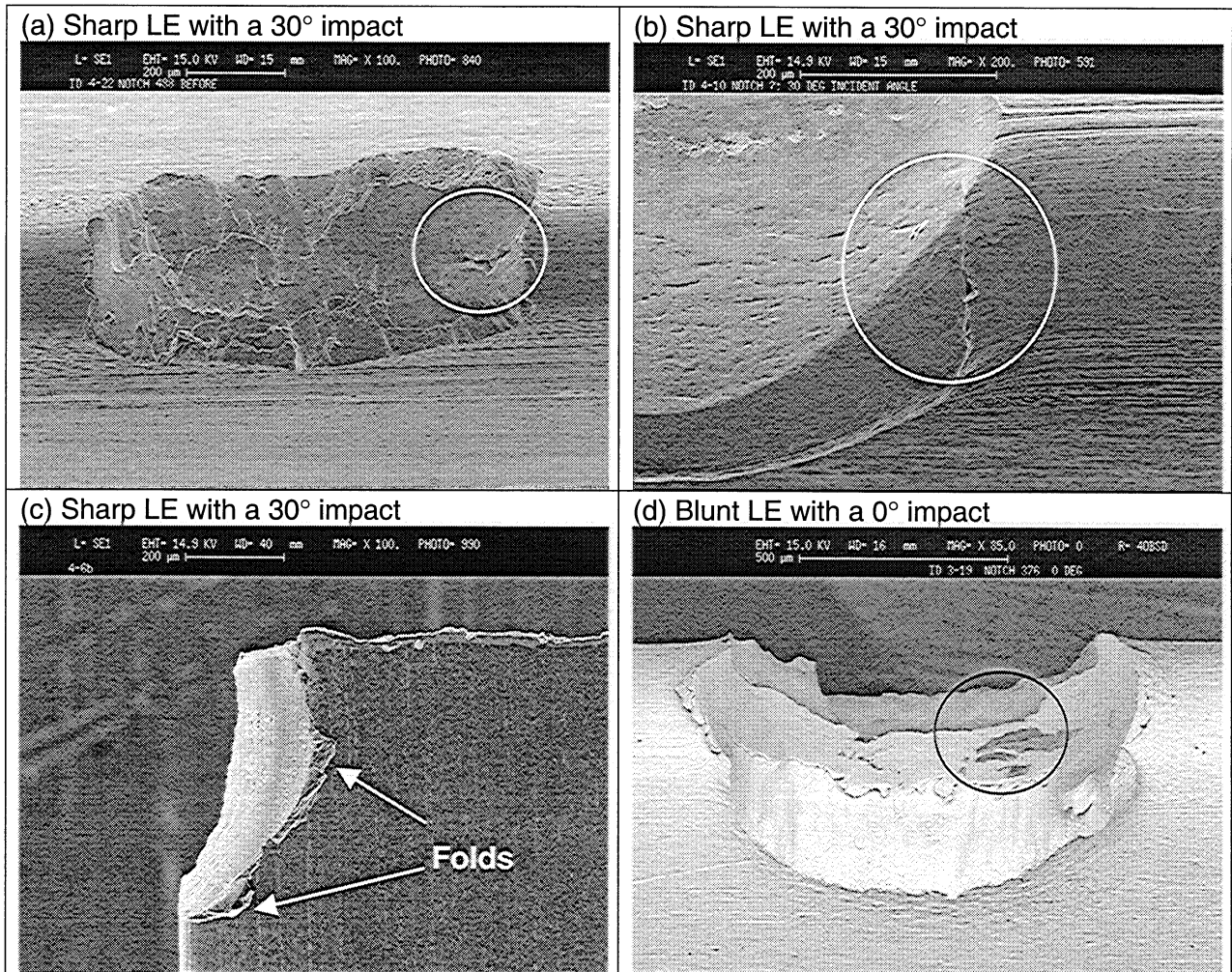


Figure 37: Other damage features: a) material shear; b) material shear; c) material fold; d) embedded glass, backscatter detector mode

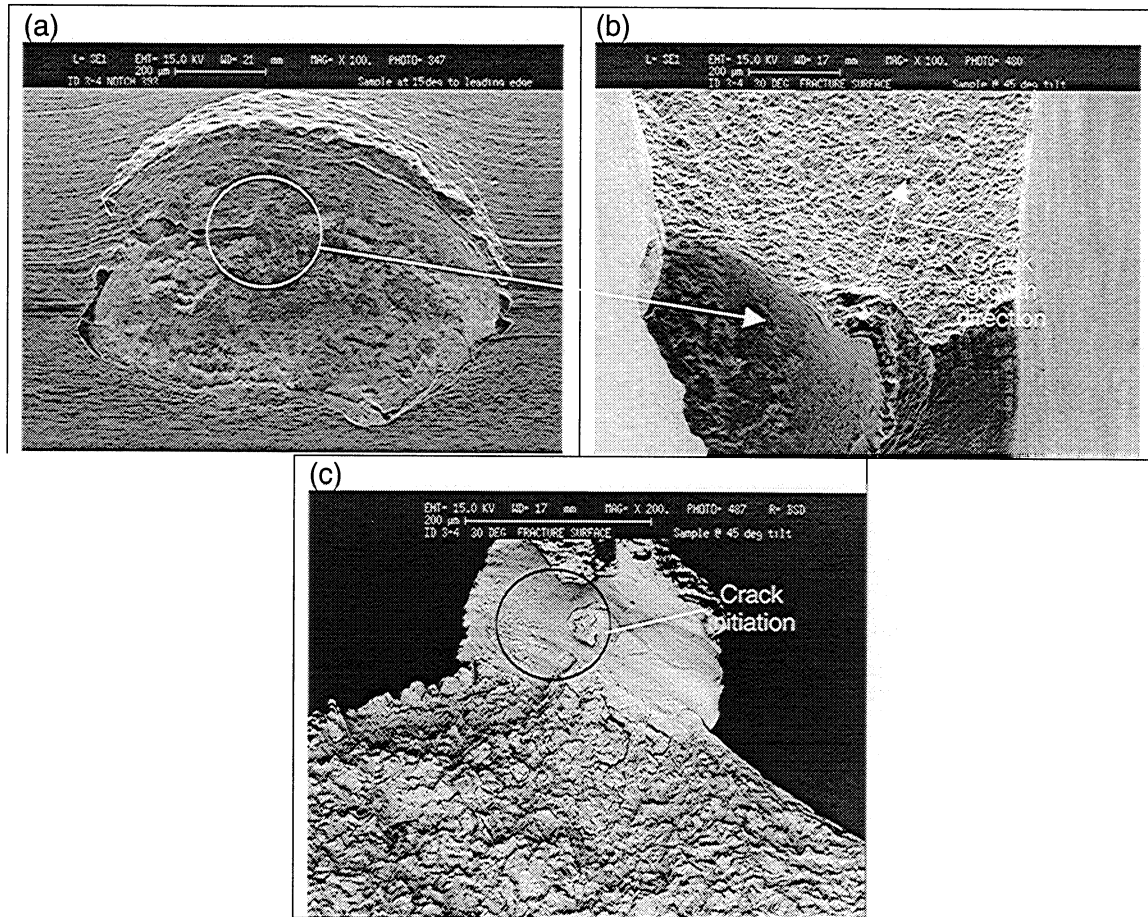


Figure 38: Shearing: a) Before fracture picture of sample 3-4 with a blunt LE and a 30° impact, material shear parallel to LE b) After fracture photo; c) After fracture photo behind material shear

### **3.3 Initiation Location in the Impact Notch**

Previous research shows that fatigue failures of samples ballistically damaged with larger steel balls at similar velocities failed at the edge (rim) of the notch<sup>7,10</sup>. Data in the present research program found that failure generally occurred in the central region of the notch (indicated by the 0.25-0.50 region in Figure 39). Regardless of the condition (notch depth, LOM, shearing, or embedded glass) of the notch, failure occurred at or near the center of the notch for 30° impacts. There is no clear correlation for 0° impacts, partially due to data scatter and a limited number of data points, as seen in Figure 40. The difference in the failure sites between this and previous work may be due to the heavier ball that was used and the resulting impact damage in the case of the previous studies. In addition, Ti-6Al-4V flat specimens were used in the previous research and were impacted on the flat surface of a larger fatigue specimen as opposed to this investigation in which thin samples were impacted on the edge; the latter being more representative of an actual airfoil edge.

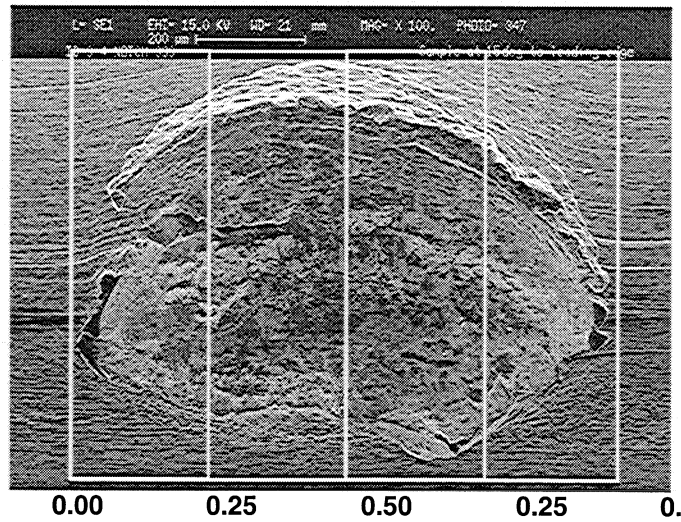


Figure 39: Crack Initiation Location photograph

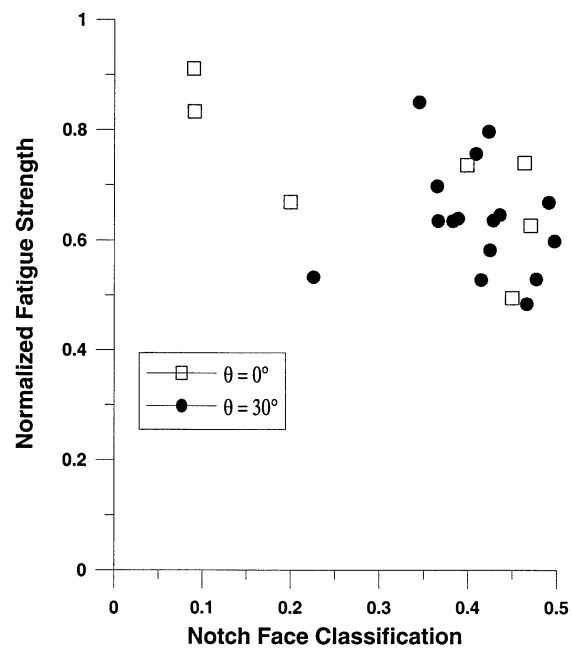


Figure 40: Crack Initiation Location

#### 4. CONCLUSIONS

High-cycle fatigue testing showed fatigue strength degradation as a result of the impact-induced edge-damage. The following sample edge-damage features were characterized using an SEM: the notch depth, loss of material (LOM) on the notch surface, material shear, material folding over the LE, and embedded glass from the shattered beads. Residual stresses that appear to play a role in fatigue strength degradation. However, damage in the impact zone seems to play a more significant role in fatigue life degradation. Samples with a 30° impact generally had a higher fatigue strength debit than those with 0° impacts. Fracture initiation generally occurred at the deeper of the pair of notches for most of the samples, both 0° and 30° incident angle. In addition, initiation generally occurred at the deeper section of the notch. However, the notch depth of the failed notch had no direct effect on the fatigue strength. Loss of material for 30° impacts showed highly scattered results indicating that LOM alone has no effect on the fatigue strength. The data for the 0° impacts, on the other hand, did show a general trend where the larger the material loss, the lower the fatigue strength. Additional testing of 0° impacts is needed to verify this trend. Samples generally failed at the notch with LOM: 81% of the 30° impacted samples failed at the

notch with LOM, and 75% for the 0° impacted samples. Even though LOM itself can not be correlated to fatigue strength debit, the result of such damage produced sharp edges and micro-folds on the surface of the notch, which could provide suitable sites for crack initiation. The same is true for material shear and folds, but not for embedded glass. Regardless of the condition (notch depth, LOM, shearing, or embedded glass) of the notch, failure occurred at or near the center of the notch for 30° impacts, but there is no clear correlation for 0° impacts, partially due to data scatter and a limited number of data points. Precision micro-sectioning showed shear bands which are oriented parallel to the applied loading direction (perpendicular to eventual fatigue cracking and the impact direction). The role of these shear bands on fatigue strength is believed to be benign, but further research is being conducted.

It is apparent that the fatigue strength of simulated blades is reduced by impacting with glass beads, which simulates FOD in engines. As the 30° incident angle represents a more typical engine FOD condition, the lower fatigue life of these impacts should be looked at with great concern. There are many more factors than damage depth which play a role in the degradation of this fatigue strength. Even though the damage features discussed are not directly correlated to the debit in fatigue strength, their presence provides suitable crack initiation sites, which could decrease the life of the blade.

## **5. SUGGESTED FUTURE RESEARCH**

A great amount of insight has been gained from this research; however, there are many areas where additional research is still required. A larger sample pool is needed to verify some of the trends seen in this research. These trends include the greater fatigue strength debit found in blunt LE samples over the sharp LE samples; the effects of residual stresses on fatigue strength, and the effects of loss of material on 0° impacted samples. In addition, the initiation site of notch-failures should be investigated to provide insight into the nature of crack initiation of ballistically impacted DCT specimens.



## 6. REFERENCES

1. Nicholas, T. "Critical Issues in High Cycle Fatigue, "International Journal of Fatigue: Vol. 21", February 1999, pp 221-231.
2. Technical Orders 1F-16CJ-2-70FI-00-1 for the F110-GE-129 engine. pp 10-41 – 10-84
3. Lanning, D.B., Haritos, G.K., and Nicholas, T. "Notch Size Effects in HCF Behavior of Ti-6Al-4V," Int. J. Fatigue, 21, 1999, pp. 643-652.
4. Personal communication from TSgt David Harrington, 20th Fighter Wing FOD Prevention NCO, Shaw AFB, to Capt. Christine Martinez, Air Force Institute of Technology. February 14, 2000.
5. Visual Data. [http://video-data.com/fiberscopes\\_borescopes.htm](http://video-data.com/fiberscopes_borescopes.htm) March 14, 2000
6. UXR. <http://www.borescope.com>. March 14, 2000
7. General Electric Aircraft Engines. AE-3326 (5/94). Advertisement pamphlet.
8. Hamrick, Joseph L., Major, USAF. "Effects Of Foreign Object Damage From Small Hard Particles On The High-Cycle Fatigue Life Of Ti-6Al-4V". PhD Dissertation. Air Force Institute of Technology. September, 1999
9. Peters, J. O., Roder, O., Boyce, B. L., Thompson, A. W., and Ritchie, R. O., "Role of Foreign Object Damage on Thresholds for High-Cycle Fatigue in Ti-

- 6Al-4V,” Metallurgical and Metals Transaction A, 1999 (submitted for publication)
10. Ruschau, J., Nicholas, T., and Thompson, S. “Influence of Foreign Object Damage (FOD) on the Fatigue Strength of Simulated Ti-6Al-4V Airfoils”. Submitted to the International Journal of Impact Engineering. April ‘00.
  11. Personal communication, Dr. Richard Bellows, Allied Signal Engines. October 7, 1997.
  12. Eylon, Daniel. “Summary of the Available Information on the Processing of the Ti-6Al-4V HCF/LCF Program Plates”. Internal Document. 1998.
  13. Bellows, R., Smith, P., Shepard, M., Eylon, D.,”Step Test, Stress Ratio and Surface Effects on the High Cycle Fatigue Behavior of Ti-6Al-4V”. Proceedings of the 4<sup>th</sup> National Turbine Engine High Cycle Fatigue Conference . Monterey, CA, February 19, 1999.
  14. Personal communication, Dr. Theodore Nicholas, Air Force Research Laboratory, Materials & Manufacturing Directorate. March 23, 2000.
  15. Weeks, C. “FOD Analytical Modeling - FOD Event Modeling”. Allison Advanced Development Company Indianapolis, Indiana. Submitted August 31, 1999. unpublished research
  16. Metal Improvement Company. “Shot Peening Applications”. 7<sup>th</sup> Ed. Internal document.

17. Maxwell, D., and Nicholas, T., "A Rapid Method for Generation of a Haigh Diagram for High Cycle Fatigue, "Fatigue Fracture Mechanics: 29<sup>th</sup> Vol., ASTM STP 1321, T.L. Panotin and S.D. Sheppard, Eds., American Society for Testing and Materials, 1999, pp. 26-641.
18. Personal communication, John Ruschau, UDRI. February 14<sup>th</sup>, 2000.
19. Personal communication, Robert Wheeler, Air Force Research Laboratory, Materials & Manufacturing Directorate. April 12, 2000

## APPENDIX

### A: Raw Data

Table 4: Sample data

Sample Code	I.D.	Max Goodman	NMGs smooth bar	Notch Failure	Section A			Section B			
					a (μm)	b (μm)	h (μm)	a (μm)	b (μm)	h (μm)	Max Depth h (μm)
051-0-1	4-1	420.41	0.74	y	319	413	107	369	594	101	107
051-0-2	4-3	380.00	0.67	y	127	173	192	507	692	192	192
051-30-1	4-13	300.00	0.53	y	581	500	323	412	517	284	323
051-30-2	4-23	275.00	0.48	y	415	341	240	475	450	213	240
051-30-3	4-6	360.95	0.64	y	312	309	144	540	362	159	159
051-30-4	4-9	340.00	0.60	y	470	344	334	475	363	353	353
051-30-5	4-11	360.78	0.64	y	680	343	427	422	398	427	427
051-30-6	4-22	396.52	0.70	y	318	412	238	553	412	272	272
sr-051-30-1	4-25	450.5	0.79	y	966.0	508.0	270	205			
sr-051-30-2	4-19	396.40	0.70	y	345		194	385			
055-0-1	4-5	562.67	0.85	n	n/a	n/a	n/a	n/a	n/a	n/a	n/a
055-0-2	4-2	601.29	0.91	y	638	564	186	63	267	186	186
055-30-1	4-7	426.56	0.65	y	563	413	200	435	390	200	200
055-30-2	4-10	528.66	0.80	n	n/a	n/a	n/a	n/a	n/a	n/a	0.0000
055-30-3	4-21	526.04	0.80	y	534	394	265	392	379		265
sr-055-30-1	9-1	456.50	0.69	y	513	453	216	481			
151-0-1	3-19	281.14	0.49	y	671.0	664.0	270.0	549.0	630.0	273.0	273
151-0-2	3-9	418.28	0.74	y	575.0	624.0	203.0	382.0	597.0	192.0	203
151-30-1	3-13	302.63	0.53	y	524.0	617.0	210.0	153.0	154.0	210.0	210

Sample Code	I.D.	Max Goodman	NMGs smooth bar	Notch Failure	Section A			Section B			
					a (μm)	b (μm)	h (μm)	a (μm)	b (μm)	h (μm)	Max Depth h (μm)
151-30-2	3-15	379.70	0.67	y	450.0	726.0	99.5	434.0	616.0	82.2	100
151-30-3	9-5	330.80	0.58	y	576.0	643.0	72.6	780.0	713.0	169.0	169
151-30-4	9-6	300.69	0.53	y	420.0	601.0	116.0	383.0	568.0	140.0	140
sr-151-30-1	3-21	453.8	0.80	y							
sr-151-30-2	3-22	538.9	0.95	n							
155-0-1	3-10	413.70	0.63	y	450.0	750.0	180.0	400.0	750.0	172.0	180
155-0-2	3-11	549.89	0.83	y	500.0	700.0	68.0	50.0	0.0	0.0	68
155-30-1	3-14	501.00	0.76	n	n/a	n/a	n/a	n/a	n/a	n/a	0.0000
155-30-2	3-16	422.23	0.64	y	462.0	606.0	212.0	294.0	398.0	157.0	212
155-30-3	3-4	420.00	0.64	y	375.0	700.0	182.0	500.0	700.0	151.0	182
155-30-4	9-2	561.37	0.85	y	475.0	700.0	161.0	250.0	700.0	0.0	161
155-30-5	9-4	499.56	0.76	y	325.0	600.0	86.9	225.0	600.0	87.0	87
sr-155-30-1	3-23	455.9	0.69	y	250.0			400			
sr-155-30-2	3-26	607.2	0.92	n							

## B: Energy Dispersive Spectroscopy

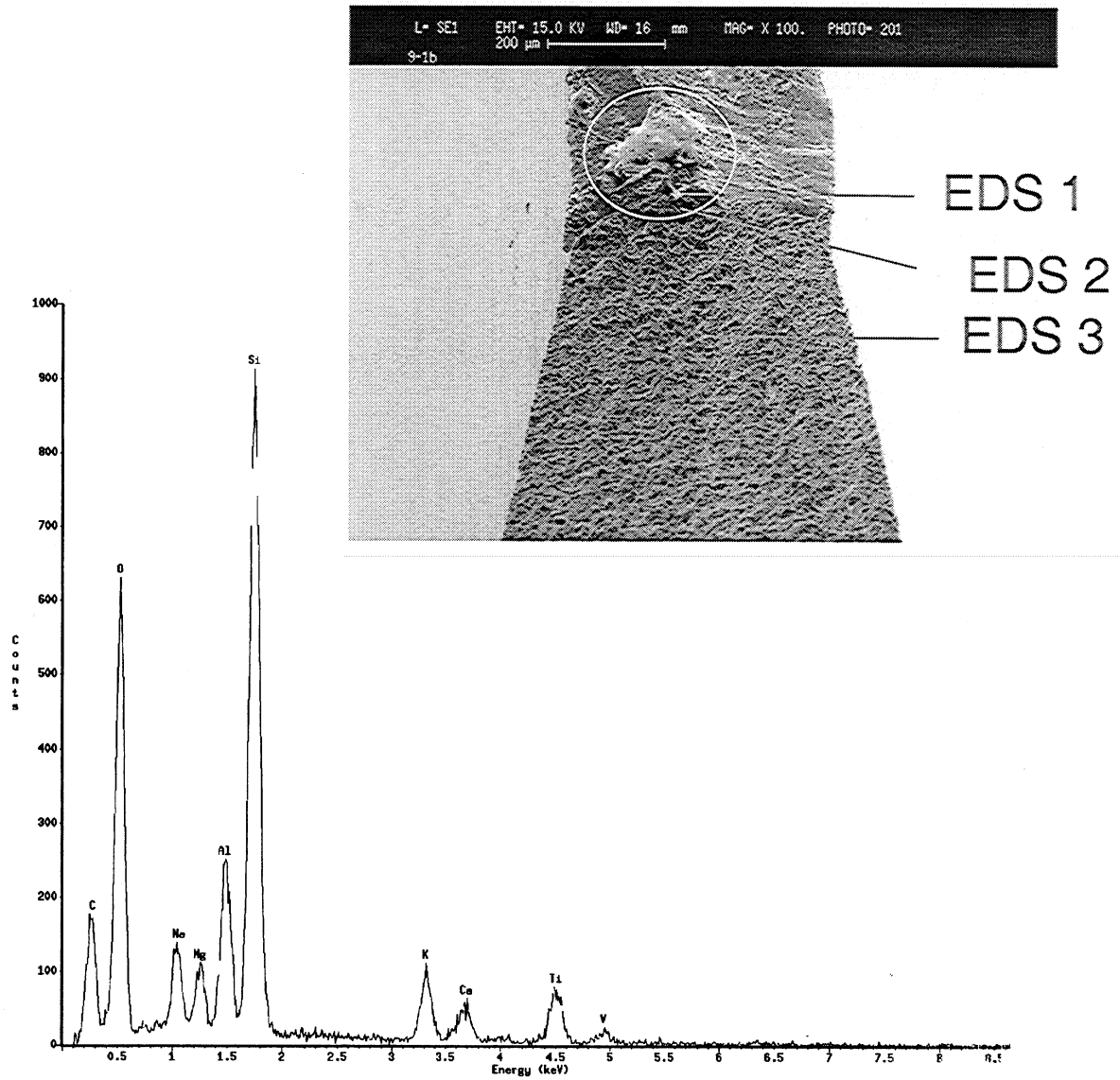


Figure 41: EDS 1, on glass of sample 4-19, 30° impact on sharp LE.

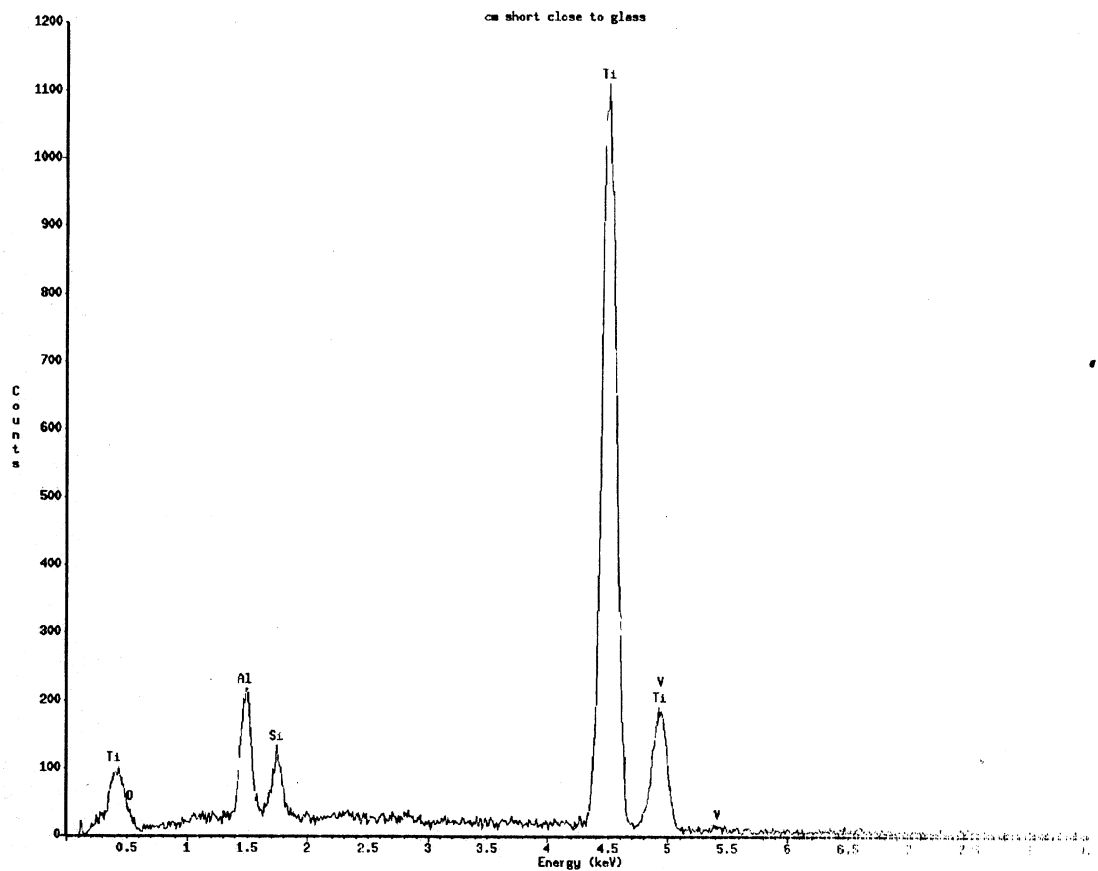


Figure 42: EDS 2; 5  $\mu\text{m}$  into the titanium alloy, away from the glass; 30° impact on sharp LE.

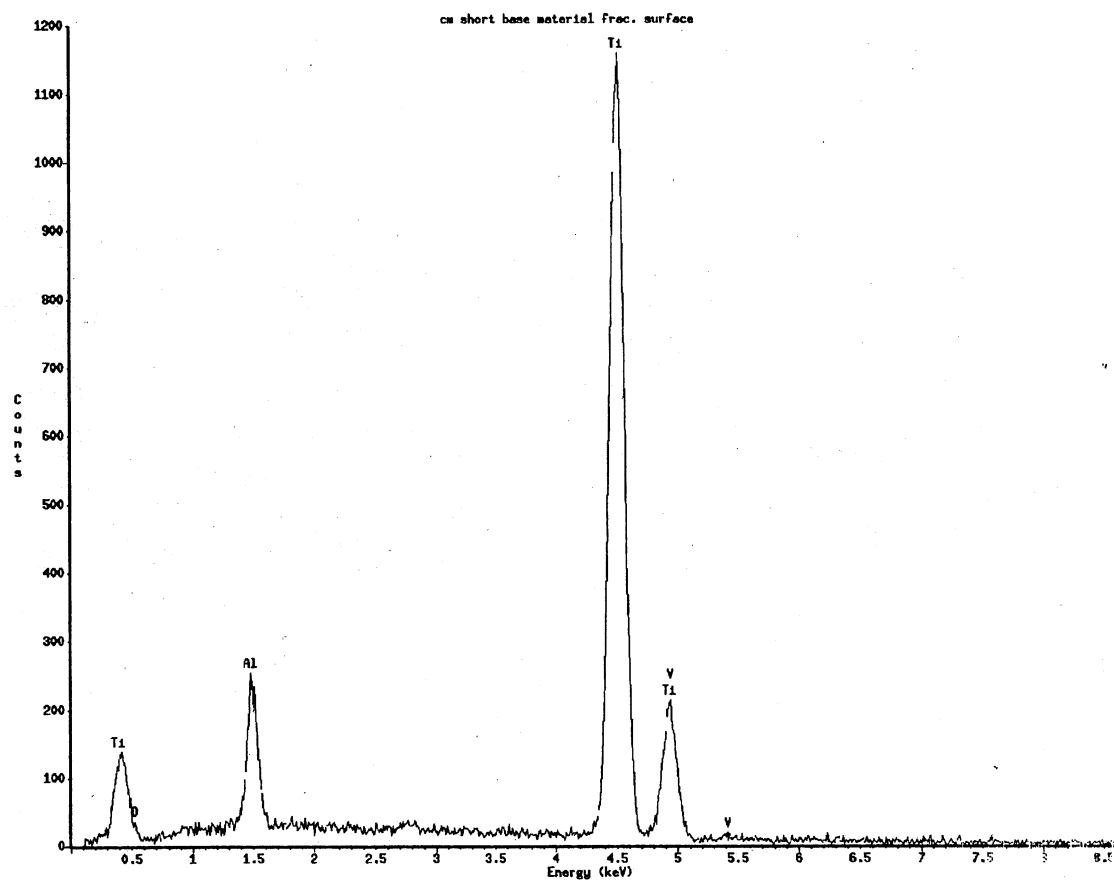


Figure 43: EDS 3; 100 $\mu$ m into alloy; 30° impact on sharp LE.





